MASTER

MONTHLY & QUARTERLY DISTRIBUTION LIST
TASK 3

DOE/SF/78003--T10

DE82 005380

U.S. Energy Research and Development Administration - RDD

1 - Deputy Director, Division of Reactor Research and Development
1 - Assistant Director, Technology
1 - Assistant Director for Reactor Safety
1 - Assistant Director for FFTF Project
1 - Assistant Director for Demonstration Plant Project
1 - Assistant Director for LMFBR Programs
3 - Chief, Fuel Systems
1 - Chief, Fast Reactor Safety
1 - Chief, Engineering & Components Development
1 - Chief, Reactor Systems, FFTF Project
1 - Chief, Reactor Systems, DEMO Plant Project
1 - Chief, Materials Development
1 - Chief, Fuel Process Engineering & Procurement

U.S. Energy Research and Development Administration - Operation Offices

1 - Project Director, Reactor Development Projects Office, Richland Operations Office
1 - Manager, Chicago Operations Office
1 - Manager, San Francisco Operations Office
1 - Manager, Oak Ridge Operations Office

Argonne National Laboratory

3 - Associate Division Director, Applied Technology Programs, Materials Science Division
2 - Associate Division Director, Analysis, EBR-II Project
1 - Associate Division Director, Materials, EBR-II Project

Atomics International

3 - Manager, LMFBR Programs
2 - Manager, Materials Engineering

Hanford Engineering Development Laboratory

1 - Vice President, Materials
1 - Vice President, Engineering
1 - Vice President, FFTF Project Management
1 - Manager, Reactor & Safety Engineering
2 - Manager, Fuels
2 - Manager, Materials Engineering
2 - Manager, Applied Research
1 - Manager, Core Engineering
1 - Manager, Mech Metallurgy
1 - Manager, Materials Analysis
1 - Manager, Materials Applications
1 - Manager, Mechanical Properties
2 - Manager, Performance Prediction
2 - Manager, Component Testing

Gulf General Atomic

2 - Manager, GCFR Fuel Element Design & Development Dept.

see letter Dec. 6, 1976 893/3/8-1

DISCLAIMER

TASK 3 DISTRIBUTION LIST (Con't)

Holifield National Laboratory

3 - Director, Metals and Ceramics Division
1 - Manager, LMFBR Fuels and Materials

Westinghouse - Advanced Reactors Division

2 - Manager, Technology
2 - Project Manager, FFTF Project
2 - Project Manager, LMFBR Demonstration Plant
1 - Manager, Fuel & Removable Assembly Design
1 - Manager, Reactor Analysis & Core Design
1 - Manager, Fuel Materials Technology

DOE/SF/78003--T10

REFERENCE FUEL STUDIES
EIGHTH QUARTERLY REPORT
AUGUST-OCTOBER 1976

Approved: C R Craig for
Manager
Reactor Engineering Section

Approved: P E Bohaboy
P. E. Bohaboy
Program Manager

November 1976

ATO3-76SF 78003

Prepared for the
U. S. Energy Research & Development Administration
under Contract No. E(04-3)-893
Task 3

FAST BREEDER REACTOR DEPARTMENT GENERAL ELECTRIC COMPANY
SUNNYVALE, CALIFORNIA 94086

DOE/SF/78003--T10

NOTICE

This report was prepared as an account of work sponsored by the United States Government. Neither the United States nor the United States Energy Research & Development Administration, nor any of their employees, nor any of their contractors, subcontractors, or their employees makes any warranty, express or implied, or assumes any legal liability or responsibility for the accuracy, completeness or usefulness of any information, apparatus, product or process disclosed, or represents that its use would not infringe privately owned rights.

TABLE OF CONTENTS

		Page
ABSTRACT		iv
SUMMARY		v-viii
1.	FUEL ROD CHEMISTRY AND THERMODYNAMICS	1-1
1.1	Fuel-Fission Product-Cladding Chemical Interaction (Subtask A)	1-1
1.2	Coolant-Fuel Chemical Interaction (Subtask B)	1-7
1.3	Migration of Fuel Components in Temperature Gradients (Subtask C)	1-9
2.	FUEL ROD ENGINEERING	2-1
3.	FUELS IRRADIATION TESTING AND ANALYSIS	3-1
3.1	High Burnup Irradiations	3-1
3.2	Low Power Irradiations	3-4
3.3	Breached Cladding	3-44
3.4	High Cladding Temperature Irradiations	3-44
3.5	Thermal Performance Irradiations	3-56
3.6	Run-To-Cladding Breach Irradiations	3-59
3.7	Subtasks B and C	3-59

ABSTRACT

In FY-76, Task 3 of Contract E(04-3)-893 consisted of the following programs:

1. Fuel Rod Chemistry and Thermodynamics (189 No. SG001)
2. Fuel Rod Engineering (189 No. SG008)
3. Fuel Irradiations Testing and Analysis (189 No. SG009)
4. Reference Structural Materials (189 No. SG044)

Starting in FY-77, the Fuel Rod Engineering Program was reorganized into other existing G.E. programs under the E(04-3)-893 contract. Continuation of the reports on technical progress of this program can be found under 189 No. SG009, Task 3, or 189 No. SG023, Task 11.

In accordance with instructions received from ERDA-RDD in January, 1976, progress reports on the Reference Structural Materials Program are now found in the Reference Cladding and Duct (RCD) monthly and quarterly status reports issued by HEDL.

Previously published results from these programs can be obtained in the following General Electric documents:

GEAP-12533, August 1974
GEAP-10028-51, August 1974
GEAP-14032-1, November 1974
GEAP-14032-2, February 1975
GEAP-14032-3, August 1975
GEAP-14032-4, January 1976

SUMMARY

189 No. SG001 - FUEL ROD CHEMISTRY AND THERMODYNAMICS

Irradiation of the second instrumented CAI capsule (CAI-2) in the GETR was completed. Post-irradiation examination of the Cs,Te-doped mini rods has shown that all four rods were intact after irradiation and little, if any, cladding component mass transport occurred.

A topical report entitled "Recent Advances in the Delineation of the Mechanism of Fission Product-Induced Intergranular Attack in Type-316 Stainless Steel Cladding" was completed.

Isothermal capsule experiments with Type 316-SS cladding and simulated fission product (Cs,Te)-fuel mixtures have been used (a) to measure the intergranular penetration rate at low oxygen activity in the absence of carbon (725°) and (b) to show that localized concentrations of carbon do not markedly catalyze Cs,Te-induced intergranular attack of 316SS at "intermediate" oxygen activity levels.

A new series of isothermal capsule experiments, designed to characterize the FCCI behavior of different Core 1 AISI 316SS cladding lots under out-of-pile conditions, is in progress. The principal test objective is to determine whether second phases produced in these alloys by various aging treatments influence subsequent fission product-induced chemical attack.

Cesium has been shown to interact chemically with Nb buffer oxidation products under typical fuel rod conditions. The stability of the resulting Cs_xNbO_y compound appears to be only slightly less than that of Cs-fuel compounds. This interaction will effectively extend the oxygen buffering capacity of niobium cladding attack inhibitors.

A high temperature solid electrolyte galvanic cell apparatus was constructed for the planned HEDL-GE oxygen potential-O:M measurements on near-stoichiometric fuel. Bench-top tests have demonstrated that the cell gives theoretical (thermodynamic) performance over the required ranges of temperature (700-1000°C) and $\Delta\bar{G}_{O_2}$ (Ni-NiO to Mn-MnO).

A memo report that reviews current knowledge of mixed (U,Pu) oxide fuel "solubility" in liquid sodium and outlines methods and approaches being employed to characterize the dispersal/solubility behavior of fuel in alkali metal coolants was prepared. An axial temperature gradient experiment, in which a column of powdered $UO_{2.03}$ and liquid sodium was heated in a 600-1000°C thermal gradient for 1000 hours, was completed. Preliminary analysis of the post-test radiographs indicates that the fuel column did not densify.

Metallographic examination of the Series IX cesium thermomigration capsules was completed. Significant and circumferentially non-uniform pellet expansion/cladding strain was observed in the UO_{2+x} blanket of the $UO_{2.02}$-$U_{0.75}Ce_{0.25}O_{2-y}$ capsule at the location of the Cs-137 peak (T≈670°C).

Some principles have been established for predicting the behavior of cesium in irradiated fuel rods based on the results of ex-reactor experiments and post-irradiation examinations of irradiated fuel rods. This information will be used to develop a basic three-dimensional Cs transport model.

SUMMARY

189 NO. SG009 - FUELS IRRADIATION TESTING AND ANALYSIS

- Diametral profilometry measurements have been made at HFEF on the 19.5% burnup, 1.3 x 10^{23} n/cm^2 fast fluence, F9C-1 series rods (X143A). Diametral strains as great as 10% were observed near the peak flux plane. An even greater diameter increase (>13%) was found near the top of the core in one rod. These fuel elements are clad in annealed Type-316 steel.

- The 14% burnup, 7 x 10^{22} n/cm^2 fast fluence F9D-1 series rods (X204) have been examined at HFEF. The maximum diameter increase was 3.1% (annealed Type-316).

- The grid spaced F9E series rods (X145A) have been examined at HFEF after 11.7% burnup and 7.5 x 10^{22} n/cm^2 fast fluence. Diameter increases were less than 3% (annealed Type-316). Secondary swelling peaks were observed near the top of the core, with magnitudes that appear to be quite sensitive to cladding temperature. These rods are being shipped to LASL for further examination.

- In the encapsulated F8B rods, a midlife power increase of 100% (starting from about 6 kW/ft (20kW/m)) had little detrimental effect. There were no cladding breaches in F8B, while two breaches occurred in series FO which essentially had an equivalent power history. These experiments, however, can be distinguished on the basis of fuel parameters (higher fuel density, smaller gap, higher O:M in FO). Fuel rod swelling was small (1% maximum on the diameter) at the low fast fluence (2-3 x 10^{22} n/cm^2) of the 6% burnup F8B rods. The swelling appeared to be anisotropic, especially in the cold worked Type-304 clad rod.

- The HFEF examinations of the 6% burnup, high-cladding-temperature F11A rods (X141A) are nearly complete. The breached rod (F11A-41) showed a substantial increase in diameter (~0.001 inch) over the top three inches of core, as compared with the previous examination (X141) at 5% burnup. No other rod showed a pronounced relative diameter change. LASL has completed the destructive examinations of the three unfailed rods removed at 5% burnup. Residual fuel/cladding diametral gaps were generally 0.001 to 0.003 inch. The maximum of 0.0018 inch of intergranular attack at the inside of the cladding was observed in the hottest rod (1300°F, 700°C at start of life).

1. FUEL ROD CHEMISTRY AND THERMODYNAMICS

Cognizant Engineer - M. G. Adamson

The program is divided into three activities dealing with specific types of fuel-coolant-cladding interactions, and its intent is to develop an understanding of the total chemical behavior of LMFBR oxide fuel rods. The objective of the first activity is to delineate the conditions for intergranular attack of Type 316 stainless steel cladding by fission products released from irradiated oxide fuel. The second objective is to delineate the conditions and the behavior of the sodium-fuel reaction in the event of a breached fuel rod. The third objective is to delineate the oxygen, actinide and fission product redistribution processes to understand the degree of component transport induced by a temperature gradient and the effects of this transport on the properties of an integral fuel rod system. The knowledge of fuel rod chemistry and thermodynamics thus obtained will aid the development of methods to control the component redistribution and reaction processes which affect the lifetime and performance of LMFBR fuel rods.

1.1 FUEL-FISSION PRODUCT-CLADDING CHEMICAL INTERACTION(Subtask A)

1.1.1 Cladding-Attack Inhibition (CAI) Experiments

Irradiation of the second instrumented CAI capsule (CAI-2) in the GETR was completed. From the thermocouple traces, the cladding inner surface temperature in the four miniature fuel rods was estimated to be 625±15°C during the high power phase of the irradiation. This phase, which spanned two reactor cycles, lasted approximately 160 hours. The capsule was removed from GETR and disassembled in the Vallecitos hot cell laboratory. Prior to opening the instrumented capsule, axial gamma scans and gamma spectra were taken at selected axial locations. Since no fission products were detected outside the fueled region, it was concluded that no major failures had occurred. A puncture analysis of the helium in the inner containment showed that integrity had been maintained throughout the test. After removing the fuel rod string from the thermal dam module and cleaning off excess NaK, the fuel rods were visually inspected, gross gamma scanned and then run through a profilometer. The gamma scans indicated a slight axial mispositioning of the fuel rods in the reactor neutron flux profile, the bottom rod (VIII) showing less fission product

activity than the other three rods. The profilometer traces showed that irradiation-induced cladding diameter increases greater than 1/2 mil did not occur in any of the rods, and careful visual inspection failed to reveal any indications of cladding breaches. Three-quarter-inch long sections were cut from the center section of each rod and longitudinal metallographic specimens prepared by cutting and grinding (through 600 grit SiC). Final polishing of these specimens has been delayed due to mechanical failure of the automatic grinder/polisher. A replacement Buehler grinder/polisher has been ordered, but is unlikely to be installed before December. Visual inspection of the 2X magnification photographs of the four longitudinal fuel rod sections indicates that gross cladding component mass transport of the type observed in the first CAI test has not occurred. Very little erosion of the cladding inner surface is evident, but at this low magnification, intergranular attack cannot be discerned.

1.1.2 FCCI Mechanism (Laboratory Experiments)

A Topical Report entitled "Recent Advances in the Delineation of the Mechanism of Fission Product-Induced Intergranular Attack in Type-316 Stainless Steel Cladding" was completed. This report describes recent laboratory results from the ongoing fission product (Cs,Te)-oxide fuel-cladding chemical interaction studies and interprets them in the context of the recently-developed combined rates model of cladding attack. The main emphasis of this experimental work was the role of impurity carbon in the cladding attack mechanism (C-14 autoradiography and SEM measurements) and the influence of Cs and Te inventory and composition on intergranular attack depth. Other aspects of the work covered in the report are the influence of surface condition of the cladding (cold work, scratches, carburization), oxygen activity effects and the efficacy of oxygen buffers (Nb foil and liquid NaK).

Two series of isothermal (725°C) capsule experiments with Type-316SS cladding and simulated fission product (Cs,Te)-fuel mixtures were performed to obtain base rate data for the intergranular attack process at low oxygen activity in the absence of carbon (Series 39 and 40). Preliminary analysis of the data indicated that with an excess of Cs+Te (Cs:Te = 1.1), at an oxygen activity corresponding to VO/V_2O_3, which is just above the oxidation threshold for Cr in Type-316SS, the intergranular penetration rate of Type-316 SS is high (d_{max} = 3.9 mils in 10h, 5.7 mils in 100h, 7.9 mils in 1000h) even in the absence of carbon. The maximum depth of attack in these tests was reached after approximately 500 hours.

Another series of isothermal capsule tests designed to examine the effect of localized concentrations of carbon impurity on Cs,Te-induced FCCI at "intermediate" oxygen-activity levels (Series 41) did not yield conclusive results. After a 100 hour heat treatment at 725°C, the resulting intergranular attack immediately under, and in the general vicinity of, the strip of graphitic carbon that was baked onto the inner surface of a Type-316 SS capsule specimen was somewhat deeper and more uniform than in non-coated locations. However, the maximum attack depth in this specimen was no greater than that measured in an uncoated capsule specimen (which, however, showed greater variability in attack depth). From these results, it is tentatively concluded that carbon "impurity" does not exhibit strong catalytic effects at "intermediate" oxygen activity levels ($(Nb)_2/Nb_2O_5$ buffer). It is intended to perform similar tests at oxygen activity levels just above the oxidation threshold for Type-316 SS.

A new series of isothermal capsule experiments, designed to characterize the fission product-induced chemical attack behavior of different Core 1 AISI Type-316 stainless steel cladding lots under out-of-pile conditions, is nearing completion. Small capsules fabricated from three different lots (vendor, HEDL T-lot, and GE "reference") - both in aged condition and as-received conditions - were loaded with controlled amounts of Cs+Te plus oxide buffer mixture (Fe/FeO and VO/V_2O_3) and heat treated at 725°C for 20 hours, a time calculated to produce a significant, but not excessive, amount of intergranular/matrix reaction. The specimen heat treatments and test conditions may be summarized as follows:

ALLOY SAMPLE	CONDITION
"CORE 1" (316SS)	As Rec'd, 300H at 1400°F, 300H at 1500°F
T-LOT/HEDL (316SS)	As Rec'd, 300H at 1400°F, 300H at 1500°F
AGED 316/GE	As Rec'd,(>5000H at 1300°F)
PE16	As Rec'd, 100H at 1400°F, 400H at 1400°F
TEST CONDITIONS	20H at 725°C
	Cs: Te(excess) = 1.1
	P_{O_2} = VO/V_2O_3, $VE/V_2O_3/C$, FeFeO/C

The various heat treatments to which the alloys were subjected are known to produce second-phase precipitation in the different alloy samples and the purpose of the tests is to determine whether these second phases influence subsequent Cs,Te-induced chemical attack of the alloys. The "aged 316/GE" specimens already contain significant quantities of precipitated sigma (σ) phase, while PEI6 was included in the test matrix because earlier work had indicated that aging "sensitizes" the alloy to Cs,Te-induced intergranular attack. Samples are currently being prepared for metallographic examination following exposure to the buffered fission product mixtures at 725°C.

During some attempts to coat 316SS surfaces with small quantities of Cs-Te mixtures, specimens of dicesium telluride were prepared by direct synthesis from the elements at ~600°C. Excess cesium was distilled off under vacuum at 300°C and the resulting weight changes indicated that the reaction product was indeed stoichiometric Cs_2Te. Further treatment under vacuum at 500°C produced no additional loss of cesium. X-ray diffraction patterns of two different Cs_2Te preparations--one of which was used to dope the CAI-2 fuel pellets--were practically identical, but bore no resemblance to the diffraction pattern obtained from a commercial preparation (Cerac, Inc.). In view of previous bad experience with commercial "Cs_2Te" preparations in producing intergranular FCCI in 316SS samples, it is concluded that the commercial product is impure.

Results have been obtained from a variety of experiments designed to characterize the Cs-niobium oxide chemical interactions that may occur in high burnup fuel rods containing niobium as a cladding attack inhibitor. First, X-ray powder diffraction results from niobium oxide pellets that had interacted with cesium in previously reported Cs thermomigration experiments showed that an unidentified phase, presumed to be $CsNbO_2$ or Cs_2NbO_3 formed as a product of the reaction between Cs and NbO_2 or Nb_2O_5 at 1100-1300°C. Second, EMF cell experiments have shown that the oxygen potential established when excess liquid cesium reacts with Nb_2O_5 at 650°C is on the order of -149 kcal/mol(-624 kJ/mol.). These data indicate that the reactivity of Cs fission products with Nb oxidation products is only slightly less than its reactivity with oxide fuel (See Figure 1-1). Consequently, the thermodynamic consequences of Cs-niobium oxide chemical interaction appear to be favorable to inhibition of FCCI (i.e. this interaction would effectively extend the buffering capacity of a given quantity of Nb by reactions such as :

$$Cs + (Nb)O + [O]_{fuel} = (CsNbO_2)$$

and

$$2Cs + (NbO_2) + [O]_{fuel} = (Cs_2NbO_3)$$

Recent EMF cell results on the Cs-O, Cs-Nb-O and Cs-U-O systems are illustrated in Figure 1-1. Some oxygen activity - oxygen concentration data were obtained for solutions of oxygen (Cs_2O) in liquid cesium over the temperature range 450-650°C. By comparing results obtained for 1.4-3.7 wt% solutions of oxygen in liquid cesium with the calculated line for the Cs(ℓ)/Cs(s or ℓ) phase boundary it becomes evident that the solubility of Cs_2O in liquid cesium exceeds 70wt% at 400°C. (in descending order, the dashed lines on Figure 1-1 refer to the following equilibria:

$$2Cs(\ell) + \tfrac{1}{2}O_2 = Cs_2O(s \text{ or } \ell)$$

$$2Cs(\ell) + \langle UO_2\rangle + O_2 = \langle Cs_2UO_4\rangle$$

and $$\langle Nb\rangle + \tfrac{1}{2}O_2 = \langle NbO\rangle$$

As described previously, the results obtained for $Cs(\ell) + \langle Cs_2UO_4\rangle + \langle UO_2\rangle$ mixtures indicate that a Cs-fuel compound more stable than Cs_2UO_4 is formed in the presence of excess liquid cesium at T>600°C.

A high temperature solid electrolyte galvanic cell apparatus was constructed for the planned HEDL-GE collaborative oxygen potential-O:M measurements on near-stoichiometric mixed oxide fuel. This galvanic cell, which is based on a 7-1/2 wt% yttria-doped thoria (YDT) electrolyte, contains a coexistent Fe/FeO reference electrode and prior to installation at HEDL, it was tested in the temperature range 700-1000°C with a variety of oxygen potential standards. Theoretical (thermodynamic) performance was achieved with metal-metal oxide standards in the oxygen potential range -147 kcal/mol (Mn/MnO) to -71 kcal/mol (Ni/NiO) (at 750°C) over the desired temperature range. Final bench-top testing was performed with urania-ceria pellets which had been equilibrated with various coexistent metal-metal oxide couples.

FIGURE 1-1 EMF CELL RESULTS FOR Cs–OXIDE EQUILIBRIA

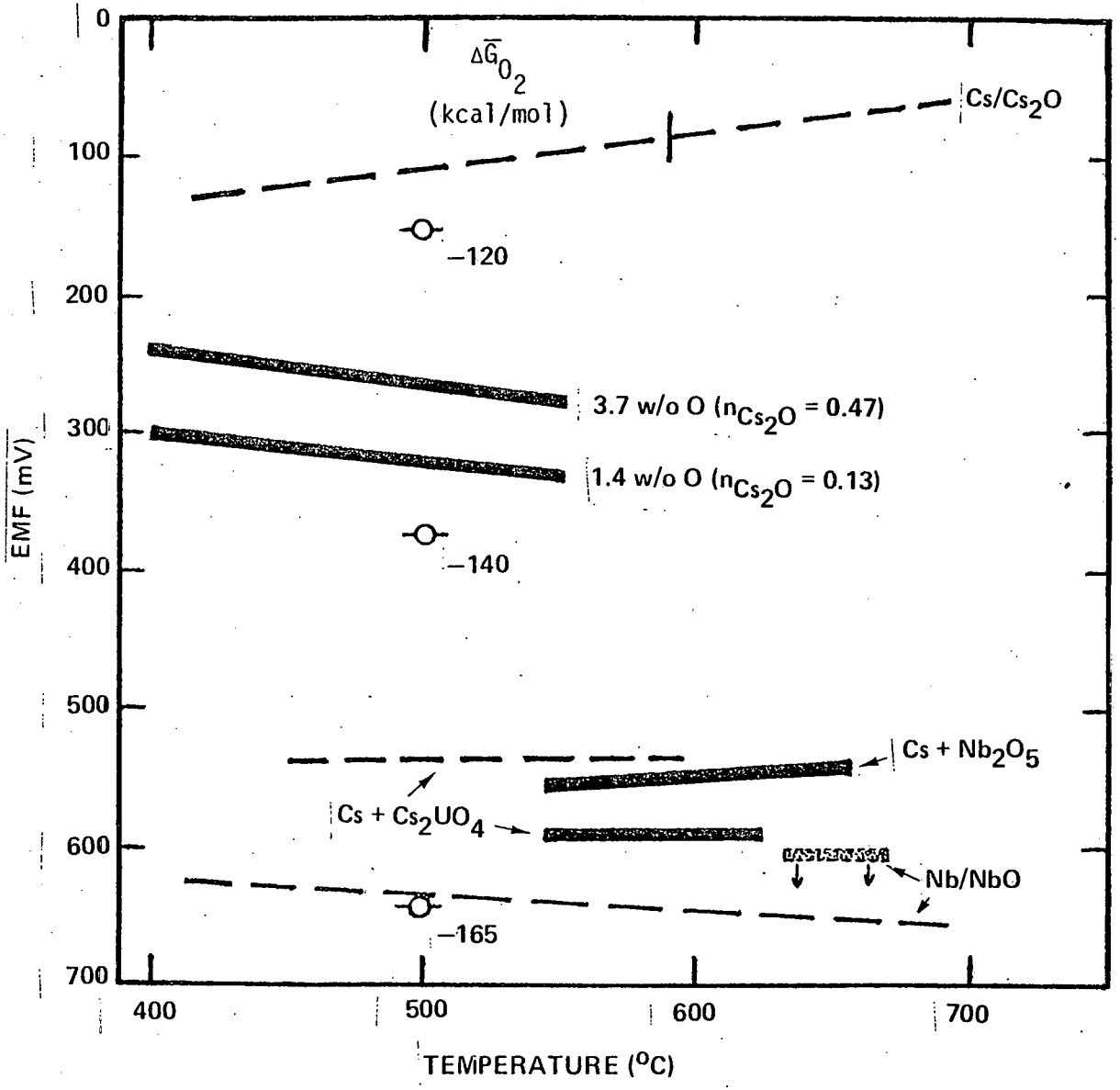

1.2 Coolant-Fuel Chemical Interaction (Subtask B)

Experiments to characterize mixed oxide fuel solubility/dispersal in liquid sodium were designed and a literature search on ceramic oxide solubility studies in liquid alkali metals was completed. This literature search was incorporated in a memo report that reviews current knowledge of mixed (U,Pu) oxide fuel "solubility" in liquid sodium and outlines methods and approaches being, and about to be, employed to characterize the dispersal/solubility behavior of fuel in alkali metal coolants (Milestone B). The main conclusion from the literature reviews is that insufficient data are presently available to determine what fraction of the fissionable material found in primary alkali metal coolant is dissolved and what fraction is in the form of suspended particles.

1.2.1 Temperature Gradient "Densification" Experiment

An axial temperature gradient experiment was performed to obtain qualitative information about the solubility of uranium oxide in liquid sodium. The rationale behind this experiment was as follows. If fuel (UO_2) shows a significant solubility in sodium in the temperature range 600-1000°C, relatively loosely packed fuel would tend to densify in cool regions in the presence of liquid sodium during prolonged equilibration in a thermal gradient. A schematic of the experimental capsule is shown in Figure 1-2. An inner molybdenum tube, 0.25 inch I.D. by 8 inches long and closed at one end was loaded initially with 30g. powdered $UO_{2.02}$ and approximately 2g. sodium. The fuel, with particle size corresponding to -100+200 mesh (particle diameters = 75-149μm), was tamped during loading to give a packing density of $\sim$7 kg/m^3 (i.e., 63.5% theoretical for UO_2). The sodium was added to the top of the packed $UO_{2.02}$ powder in the form of small beads, then the capsule was heated to 500°C under argon to allow the sodium to wet the fuel. Following this treatment, more sodium was added and the process repeated until the required quantity of sodium to fill void space in the capsule had been added. The total quantity of sodium added was far in excess of the quantity expected to react with UO_{2+x} according to the reaction

$$\frac{3x}{2}\,[Na] + \langle UO_{2+x} \rangle = \frac{x}{2} \langle Na_3UO_4 \rangle + \frac{2-x}{2} \langle UO_2 \rangle .$$

The loaded molybdenum capsule was placed inside a longer close-fitting stainless steel capsule and the gap between the two capsules filled with sodium. A stainless

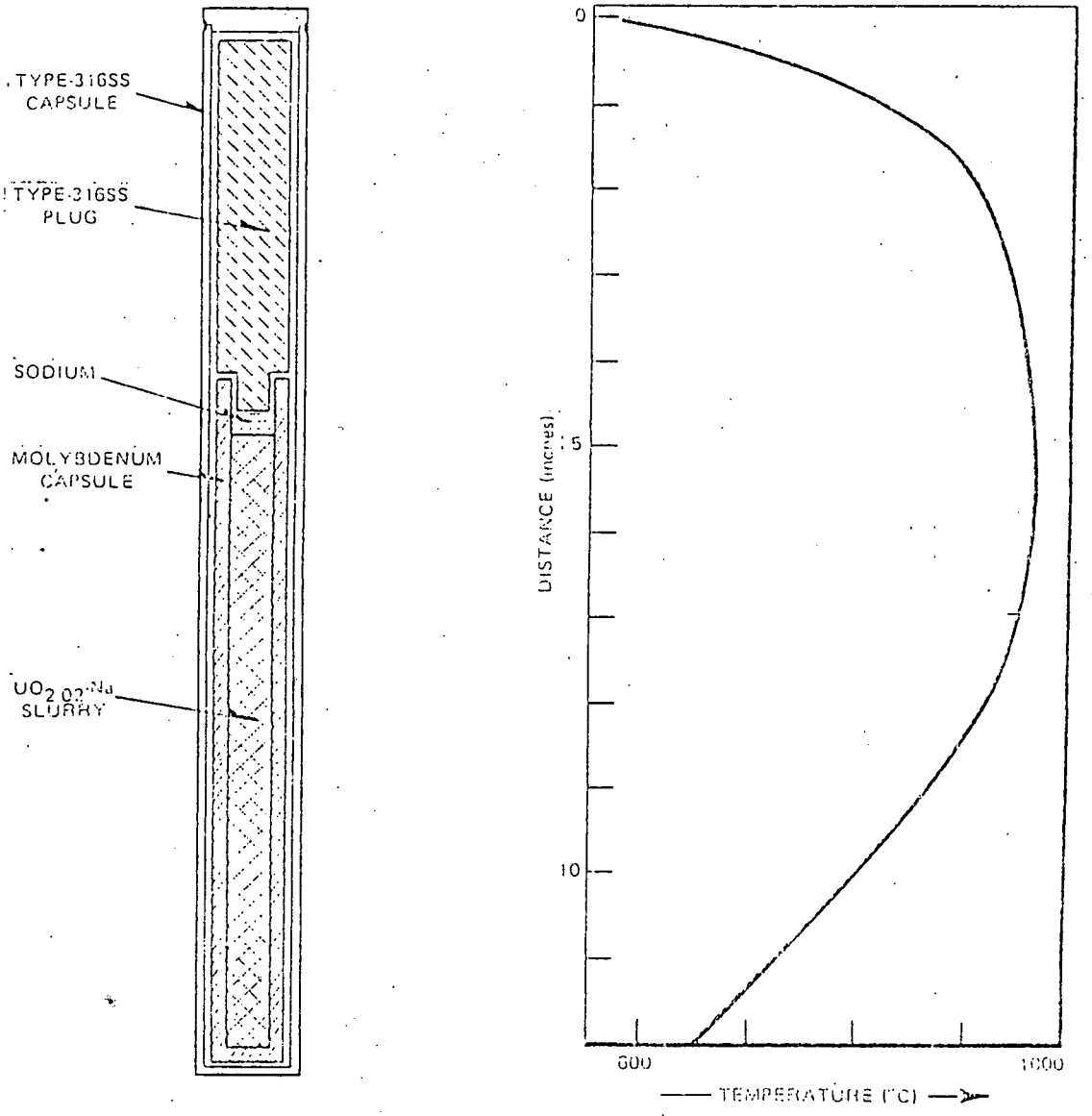

Figure 2-1 Design of UO_2-Na "Densification" Experiment

steel plug was inserted into the top of the Mo capsule to occupy the remaining void space in the duplex capsule. Final closure of the duplex capsule was made at the top end of the outer stainless steel capsule by welding under argon. Thermal gradient annealing was performed with the capsule in a vertical position inside a three-zone tube furnace. Thermocouples were strapped to the capsule at different axial locations to measure the axial temperature profile. The actual temperature profile during the experiment, which ran for 1000 hours, is also shown in Figure 2-2. Before starting the thermal gradient anneal, neutron and X-radiographs of the capsule were taken (a) to verify that the fuel column was continuous and (b) to measure the length of the fuel column. Post-test analysis has thus far consisted of radiographic examination of the intact capsule. The preliminary results indicate that the fuel column did not undergo any change in length, nor did the cooler fuel appear to densify as a result of the thermal gradient treatment. More detailed examination of the capsule is in progress.

Experiments in which ^{235}U-enriched mixed (U,Pu) oxide fuel samples will be equilibrated with pure liquid sodium while clear metal foils are simultaneously exposed to the sodium are being assembled. By employing metal frit filters in certain of the stainless steel capsules and observing/measuring deposited fuel material on the foils after various heat treatments, it is hoped to differentiate between crystallized (i.e., once dissolved) and deposited (i.e., originally suspended) fuel material. Mechanically dispersed fuel is expected to have particle sizes ranging from ca. 10μm to 100μm (i.e., these diameters correspond to single grain size in prototypical fuel pellets to the maximum particle size noted in reactors such as DFR) so filter pore sizes will be selected accordingly (e.g., 5μm to 100μm).

1.3 Migration of Fuel Components in Temperature Gradients (Subtask C)

Cesium thermomigration experiments were recently performed to simultaneously obtain rate data for the axial migration of Cs from a column of mixed oxide fuel to the urania blanket and information about fuel swelling at the mixed oxide-UO_2 interface due to Cs-fuel chemical reaction. In this series of tests (Series IX) mixed urania-cesia ($U_{.75}Ce_{.25}O_{2-y}$) pellets were used as a stand-in for urania-plutonia fuel, and two different capsule designs were employed. The basic difference in the designs was that longer molybdenum capsules were used for the tests with the highest maximum temperature and steepest axial temperature gradient (stoichiometric fuel and stoichiometric UO_2). In each case, the mixed oxide-UO_2 pellet interface was located inside

a length of Type-316SS cladding at a position corresponding to a temperature of ∿800°C; the pellet-clad diametral gap at this location was ≈ 3 mils. The evolution of the cesium gradients in the four test capsules was illustrated in Figure 1 (molybdenum capsules no's 1 and 2) and 2 (316SS capsules no's 3 and 4) of the February-April 1976 Quarterly Progress Report for Task 3, 189 No. SG001.

Metallographic examination of the blanket and blanket-fuel interface regions of representative Cs thermomigration capsules has been completed. As previously reported, no fuel or blanket swelling was evident at the $UO_{2.00}$-$U_{.75}Ce_{.25}O_2$ interface, however, significant pellet expansion was observed in the $UO_{2.02}$ blanket of the $UO_{2.02}$-$U_{.75}Ce_{.25}O_{2-y}$ capsule at the location of the Cs peak. An interesting feature of this Cs-$UO_{2.02}$ interaction was that concomitant cladding strain (ΔD_{max} = 8 mils) varied with orientation of the rod. At certain orientations there was no measureable pellet or cladding diametral increase. This circumferentially non-uniform interaction has also been noted in irradiated fuel rods.

A paper entitled "Transport and Reactions of Cesium Fission Products in Oxide Fuel Rods" was prepared for presentation at the American Ceramic Society Nuclear Division Fall Meeting, San Francisco, October 31-November 3, 1976. In this paper, it was shown how principles for predicting the behavior of cesium in irradiated fuel rods may be established from the results of ex-reactor experiments such as the above and irradiated fuel rod tests.

Both radial and axial transport paths were considered, together with chemical reactions of Cs with fuel, cladding and other fission products. In evaluating gaseous transport mechanisms for Cs, the half-lives of the various xenon precursors were also taken into account. Figure 1-3 is a flow diagram illustrating the various processes that need to be taken into account in the development of a basic 3-dimensional Cs transport model. The "high T" and "low T" indicate fuel conditions, the "low T" side referring specifically to the cool outer rim of fuel (T<1100°C), and the fuel-cladding gap.

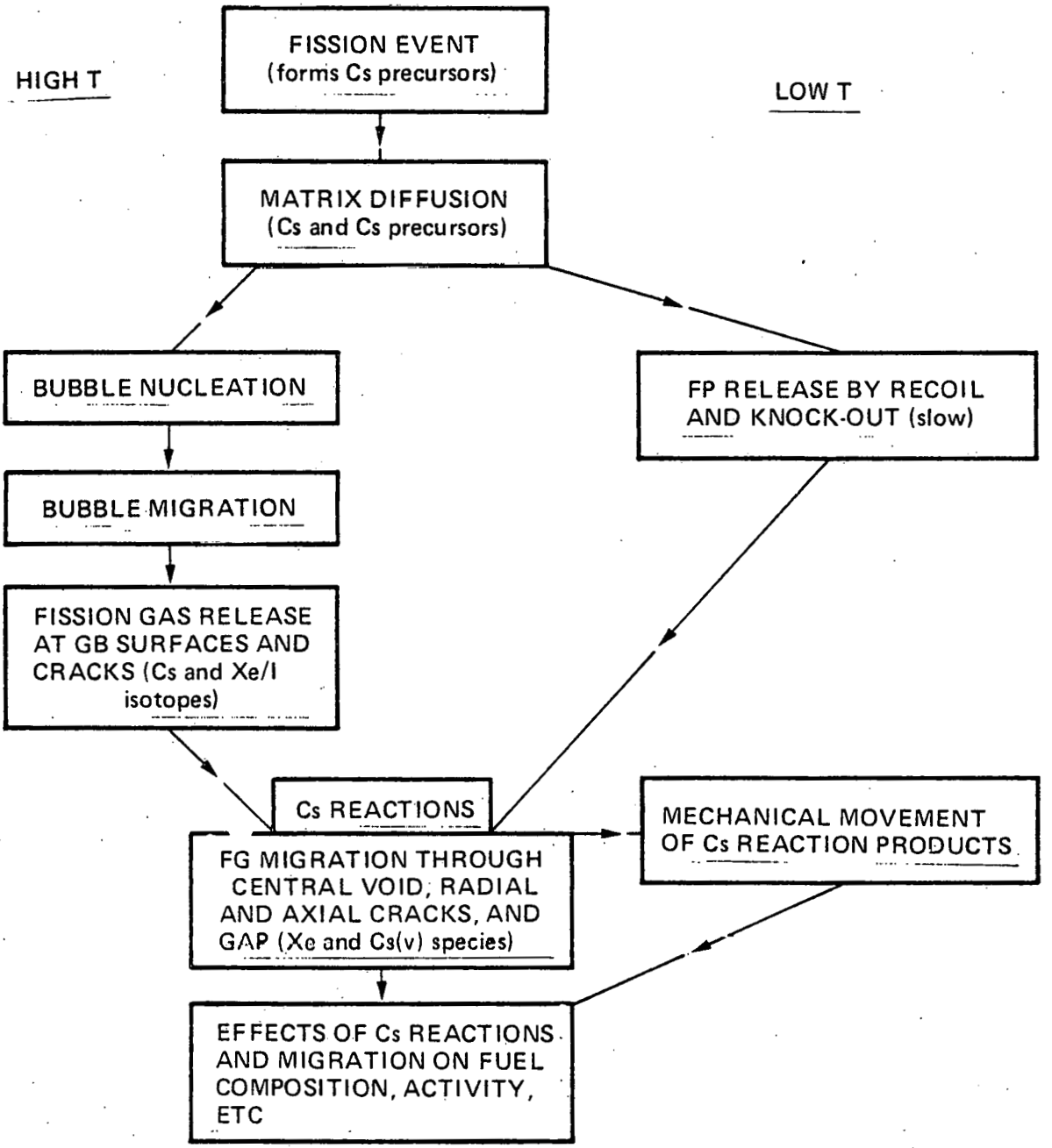

FIGURE 1-3

PROPOSED FLOW DIAGRAM FOR 3-DIMENSIONAL Cs TRANSPORT MODEL

Major Contributors

M. G. Adamson
E. A. Aitken
W. H. Reineking
J. E. Lewis
G. R. Lundeen
R. E. Smith

2. FUEL ROD ENGINEERING

Cognizant Engineer - B. L. Harbourne

Starting in FY-77 the work scope of the Fuel Rod Engineering program has been reorganized into two other existing General Electric programs under contract E(04-3)-893. The shift in work scope is shown below:

FY-76	FY-77
Subtask A - Development and Validation of Fuel Rod Design	189 No. SG023, Task 11, Core Component Design And Analysis
Subtask B - Fuel Property Design Correlations	189 No. SG009, Task 3, Fuel Irradiation Testing and Analysis
Subtask C - Structural Material Property Design Correlations	189 No. SG009, Task 3, Fuel Irradiation Testing and Analysis
Subtask D - Fuel Rod Data Analysis	189 No. SG009, Task 3, Fuel Irradiation Testing and Analysis

Future progress reports in FY-77 will be reported in the appropriate program noted above.

3. FUELS IRRADIATION TESTING AND ANALYSIS

Cognizant Engineer: W.H. McCarthy

The objective of the Fuels Irradiation Testing and Analysis Program is to determine experimentally the behavior of fuel rods under fast flux irradiation. The work is focused on supporting the core design for FTR, CRBR and PLBR. The irradiation tests provide data for development of design correlations in five general areas: High Burnup Irradiations, Low Power Irradiations, High Cladding Temperature Irradiations, Thermal Performance Irradiations, and Run to (and Beyond) Cladding Breach Tests. Table 3-1 summarizes the current status of the program. Detailed program objectives and earlier progress can be found in the annual report.(3-1)

3.1 HIGH BURNUP IRRADIATIONS

Several thirty-seven rod subassemblies of unencapsulated mixed oxide rods are being irradiated to high burnup (>100 Mwd/kg). Some of these F9 series (A-F) irradiations have had the objective of run-to-cladding breach. The earlier encapsulated high burnup experiments have completed thier irradiation.

3.1.1 F9A-1

The F9A-1 (X214) experiment began irradiation in run 81A. This is a reconstitution of (23) F9A series rods from X043A, together with (12) F9C-2 series rods from X144. Previous burnup levels were nine and ten percent, respectively, and the irradiation is expected to continue to a goal burnup in excess of sixteen percent. (The final goal burnup is pending the results of post-irradiation examinations to be carried out in GFY1977.) Peak burnup at the end of run 84 is estimated to be 15% and peak fast fluence is 9×10^{22} n/cm^2.

3.1.2 F9C-1

The leading burnup experiment, F9C-1 (X143A) achieved 19-1/2% burnup (1.3×10^{23} n/cm^2 fast fluence) at the end of run 79 (October 1975). Its objective is run to cladding breach. X143A was discharged from the reactor, not because of a cladding breach, but because of excessive metal swelling in the irradiation vehicle. Nondestructive examinations of the rods are nearly complete at

TABLE 3-1

GENERAL ELECTRIC FUELED EXPERIMENTS IN EBR-II

(October 1976 - Run 84 Complete)

SERIES	SUBASSEMBLY	NUMBER OF RODS	DESCRIPTION	IRRADIATION DATES	PEAK POWER kW/ft(a)	MAX. BURNUP % (a)	NO. OF CLADDING BREACHES	STATUS
F0	XG02,XG03,XG04	5E	Low Power, High Density	7/65-8/72	5-9	4-11	2	PIE
F1	XG01	6E	One-Run Proof	5/65	14-17	0.2	0	GEAP5770
F2	XG05,XG06,X050	21E	Fuel Rod Variables	9/65-5/70	9-16	6,7,13	3	GEAP 13538,13549
F3A	X040	16B	Initial Bare Rod (.290)	8/68-5/70	13-15	5	0	GEAP13735
F3B-ElH	X027,X151,X167,X233	18E	Fuel Variables	11/67-7/75	10-13	9,10,12	8	PIE
F4	X011,X039,X070	9E	Low Density	5/66-8/70	13-15	9	2	PIE
F5	X064,X151,X167,X233	19E	High Cladding Temp.	5/66-7/75	10-14	6,7,9	1	GEAP13971,To F20, PIE
F6	X010	4E	Rod Variables,Low Power	3/66-4/69	9	6	1	GEAP14098
F8	X019	7E	Fuel Variables, Low Power	1/67-8/69	9	5	0	GEAP14098
F8A	X020,X081	9E	Rod Variables	1/67-10/72	8-11	12	3	GEAP14126
F8B	X036,X117,X118	19E	Low Power,High Burnup	7/68-7/75	3-9	6,11	0	PIE
F9A	X043	37B	316 Clad,Fuel Variables	2/69-2/73	10-14	10	0	PIE, to F9A-1
F9A-1	X214	(37B)	F9A&F9C-2 Combined	2/76-6/77	12	4,14,15	0	In Reactor
F9B	X062	37B	Rod Variables	5/69-7/74	8-10	12	0	PIE, F9B-1
F9B-1	-	(37B)	F9B,D Power Change	8/76-10/77	9	12	0	AIP
F9C	X056	37B	316 Clad,Fuel Variables	4/69-5/71	10-12	7	0	To F9C-1,to F9C-2
F9C-1	X143	(19B)	Leading RTCB(Battleship)	2/72-12/75	11-13	19	0	Exam at EBR-II
F9C-2	X144	(19B)	F9C Continuation	2/72-7/73	10-13	11	0	PIE & to F9A-1
F9D	X058	37B	316 Clad,Fuel Variables, Low Power	4/69-9/72	7-9	8	0	PIE & to F9D-1
F9D-1	X204	(19B)	Low Power,Battleship,Xe	6/74-10/75	8-9	14	0	Exam at EBR-II
F9E	X145	37B	Grid Spaced, 316 (.250)	6/72-7/75	11-13	11	0	Ship to LASL
F9F	X155	37B	Grid Spaced,FTR Clad(.230)	10/72-4/76	10-11	12	0	Exam at EBR-II
F10A	X121	19E	High Cladding Temp.	2/72-11/73	12-14	5	2	GEAP14133,F10A-1
F10A-1	X121A	(19E)	F10A & F10B Continuation	11/75-1/77	12-14	9	-	In-Reactor
F10B	X122	19E	High Cladding Temp.	12/71-2/73	12-14	5	3	GEAP14133,F10A-1
F11A	X141	37B	High Cladding Temp.(Bare)	12/72-1/74	10-12	5	0	PIE & to F11A-1
F11A-1	-	(37B)	F11A Continuation	9/75-9/77	10-12	6	1	Exam at EBR-II
F20	X190	29E	Power to Melt	11/73-3/74	14-21	0.005,0.3, 0.7,6,9	0	PIE,GEAP14134

(a) Using Reactor Power Adjustment factors (currently 0.91)

HFEF/N. The spacing wires were very slack over the fueled lengths of the rods. The wires were removed to permit diameter profilometry and because they were too slack for reconstitution. Methods for re-irradiation are being explored. The stacked combination beam arrangement of a grid spaced assembly using MK E-19 hardware may be proposed as the most effective means for continuing this irradiation. The feasibility of this concept has been discussed with EBR-II Project personnel both in Chicago and at INEL, and the problems do not seem to be insurmountable. Specific designs and procedures remain to be worked out, however. There is some possibility that this concept may also be useful to HEDL for high fluence reconstitutions.

The outer cross sectional dimensions of the X143A subassembly were measured. The maximum across-flat dimensional increase was 0.040 inch (1 mm), equal to the allowable subassembly thickness increase. Therefore, the EBR-II calculations to determine when a Type 304 subassembly should be removed from the core are not over-conservative, and this experiment, at least, did receive as much exposure as the vehicle would allow.

The measured rod length changes are listed in Table 3-2, together with burnup and fluence data. At the previous interim examination (X143, $\sim 5.5 \times 10^{22}$ n/cm^2), there was essentially no length increase in these rods. The $\sim$3.3% length increase at 1.2×10^{23} n/cm^2 fast fluence in the Type-316 annealed rods, and $\sim$1.8% increase at 7.5×10^{22} n/cm^2 fast fluence in the Type-304 elements first irradiated in X143, suggest that the length increases are approximately linear, with an incubation fluence of $\sim 5 \times 10^{22}$ n/cm^2 and a rate of 0.5% length increase per 10^{22} n/cm^2.

Preliminary maximum diameter increase data for the X143A rods were listed in Table 3-3. They are plotted against maximum fluence* in Figure 3-1. Diameter increases as great as 0.025 inch (0.64 mm), or 10%, were observed near the peak flux plane in these Type 316 annealed clad rods. One rod (F9C-24) exhibited a very large secondary diameter peak near the top of the fuel. The indicated diameter increase there was 0.033 inch (0.84 mm, 13%) when the range of the

---

* The maximum fluence and maximum diameter positions do not, in general, coincide. This engineering presentation should not, therefore, be used to define a scientific relationship between fluence and swelling. The local fluences, temperatures and diameters will be correlated in the final presentation of the data.

TABLE 3-2

LENGTH CHANGES IN F9C-1 SERIES (X143A) RODS

ROD	PEAK BURNUP	PEAK FAST FLUENCE	CUMULATED LENGTH INCREASE, Inch (mm) AFTER X143 ($\sim 5.5 \times 10^{22}$ n/cm^2)	CUMULATED LENGTH INCREASE, Inch (mm) AFTER X143A ($\sim 1.2 \times 10^{22}$ n/cm^2)	PERCENT[a] LENGTH INCREASE AFTER X143A
F9C-1	18.8	11.9	-0.06(1.5)[b]	0.457(11.6)[b]	3.4[b]
-4	18.8	11.9	0.00	0.437(11.1)	3.2
-5	18.3	11.2	-0.02(.5)	0.442(11.2)	3.3
-9	18.5	11.5	+0.01(.2)	0.408(10.4)	3.0
-10	18.1	11.1	-0.01(.2)	0.447(11.4)	3.3
-11	19.2	12.4	+0.01(.2)	0.377(9.5)	2.8
-18	18.6	11.9	+0.01(.2)	0.433(11.0)	3.2
-20	19.1	12.3	+0.01(.2)	0.442(11.2)	3.3
-21	18.6	11.6	0.00	0.446(11.3)	3.3
-23	19.3	12.7	-0.07(1.8)[b]	0.522(13.3)[b]	3.9[b]
-24	19.0	12.3	+0.01(.2)	0.517(13.1)	3.8
-25	18.7	11.9	(c)	0.411(10.4)	3.0
-26	18.7	11.7	0.00	0.351(8.9)	2.6
-27	19.0	12.1	+0.04(1.0)	0.437(11.1)	3.2
-30	19.5	12.8	-0.01(.2)	0.455(11.6)	3.4
-32	19.5	12.8	-0.07(1.8)[b]	0.503(12.8)[b]	3.7[b]
F9C-38	19.0	12.3	-0.01(.2)	0.514(13.1)	3.8
F9A-43[d]	13.4	7.7	-0.02(.5)	0.261(6.6)	1.9
F9A-46[d]	13.2	7.4	-0.01(.2)	0.219(5.6)	1.6

a) Percent of 13.5 inch (343mm) nominal core length.
b) Bottom end plugs of rods F9C-1, -23 and -32 were trimmed slightly during interim examination following X056A. The post X143 decreases (vs. preirradiation) were, therefore, added to the total changes for these three rods for the post X143A data.
c) Post X143 measurement for F9C - 25 was clearly in error.
d) F9A - 43 and - 46 were inserted as fresh rods in X143 when remainder had ~6.2 burnup, ~4×10^{22}n/cm peak fast fluence.

TABLE 3-3 PRELIMINARY MAXIMUM DIAMETER CHANGES IN SERIES F9C
F9C-1(X143A) RODS

Rod	Max.[a] Post Irrad. Diameter Inch		Diameter Increase		Peak	
			mils	%	Burnup	Fast Fluence
	0°	90°			%	10^{22} n/cm^2
F9C-1	>.2707[b]	>.2660[b]	> 18.[b]	>7.2[b]	18.8	11.9
F9C-4	.2690	.2712	20.2	8.1	18.8	11.9
F9C-5	.2660	.2670	16.4	6.6	18.3	11.2
F9C-9	.2665	.2675	16.7	6.7	18.5	11.5
F9C-10	.2681	.2673	17.6	7.0	18.1	11.1
F9C-11	.2718	.2742	23.0	9.2	19.2	12.4
F9C-18	.2692	.2682	18.7	7.5-	18.6	11.9
F9C-20	.2715	.2720	21.7	8.7	19.1	12.3
F9C-21	.2714	.2691	20.2	8.1	18.6	11.6
F9C-23	.2720	.2743	23.2	9.3	19.3	12.7
F9C-24	.2720[b]	.2717[b]	21.8[b]	8.7[b]	19.0	12.3
F9C-25	.2706	.2717	21.3	8.5	18.7	11.9
F9C-26	.2691	.2687	18.9	7.6	18.7	11.7
F9C-27	.2705	.2730	22.1	8.8	19.0	12.1
F9C-30	.2707	.2732	21.9	8.8	19.5	12.8
F9C-32	.2750	.2753	25.1	10.0	19.5	12.8
F9C-38	.2709	.2720	21.4	8.6	19.0	12.3
F9A-43	.2593	.259	9.2	3.7	13.4	7.7
F9A-46	.2583	.2564	7.4	3.0	13.2	7.4
F9C-24[c]	>.283[b,c]	-	>33.0[c]	>13.2[c]		
F9A-43[d]	.2593	.2675[d]	13.4[d]	5.4[d]		
F9A-46[d]	.2583	.2582[d]	8.2[d]	3.3[d]		

a) Near peak flux position (except last 3 lines)
b) Suspect value - will be remeasured
c) Secondary Peak at top of fuel - beyond range of instrument
d) Sharp spikes on 90° profile
e) All type 316 Annealed cladding except F9A-43 and F9A-46 are 304 Annealed

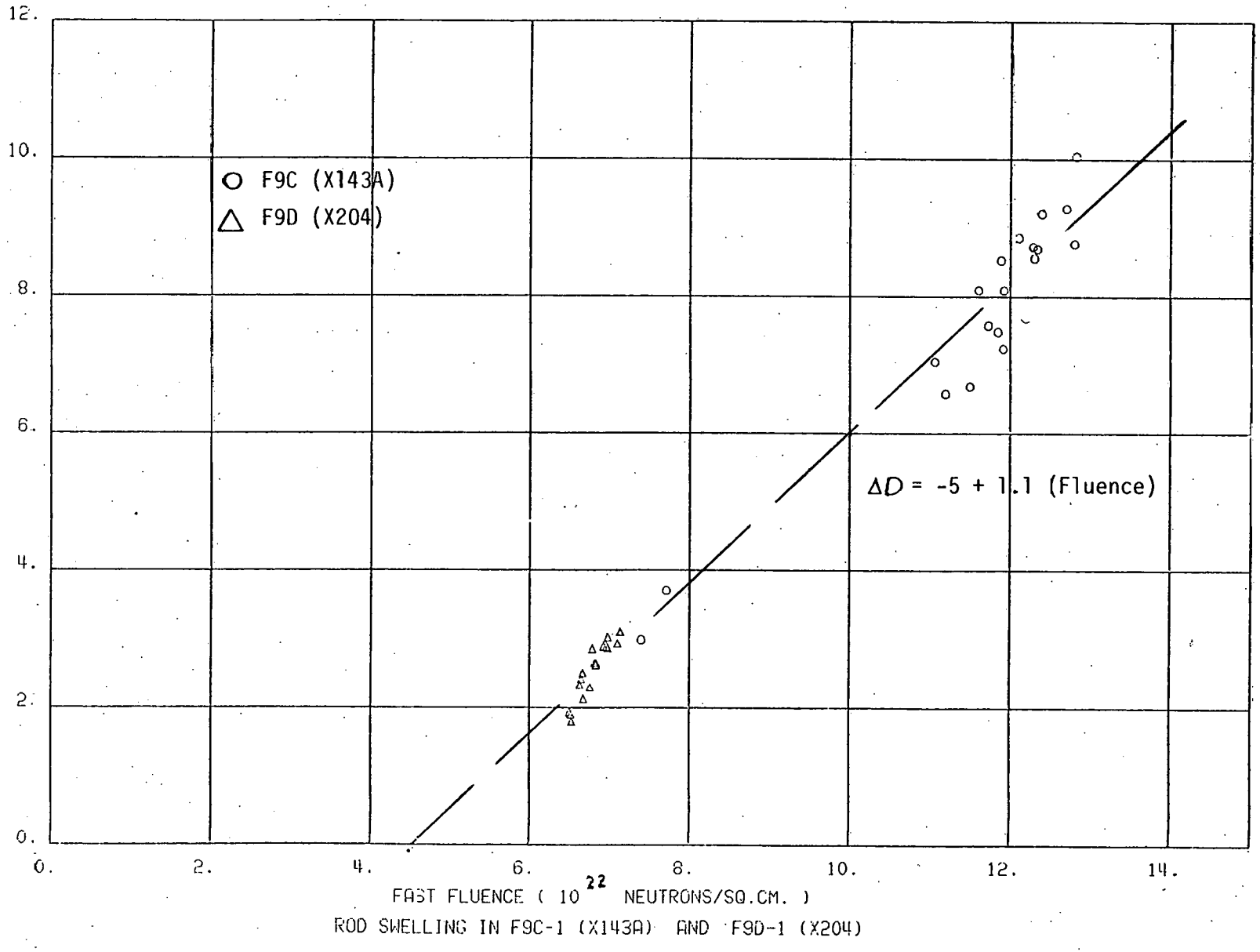

ROD SWELLING IN F9C-1 (X143A) AND F9D-1 (X204)

FIGURE 3-1

LVDT* measurement system was exhausted. Secondary peaks were also noted on several other F9C-1 series rods, but the magnitudes were less than the maximum diameter increase near the peak flux position. It is expected that the X143A secondary peaks will be included in the analysis to be performed for the F9E series (X145A), Section 3.1.4. The F9C-1 diameter profiles appear to be consistent with the length changes (6-10% for diameter and 3-4% for length), but the diameter increase profiles have not yet been integrated. The rods exhibited considerable localized bending (e.g., 0.1 inches in a 4 inch length), and neutron radiography showed several pellet-to-pellet gaps in each high fluence rod (gaps up to 0.08 inch (2. mm) long). A few rods exhibited a breaking-up of fuel pellets toward the top of the core.

3.1.3 F9D-1

The nineteen rod low power F9D-1 (X204) experiment is being examined at EBR-II following successful completion of the irradiation to its goal burnup of 14% peak (7×10^{22} n/cm^2 peak fast fluence). Subsequent to a difficult irradiation vehicle disassembly operation, the rods have been visually examined, profiled for rod diameter, and gross gamma scanned at HFEF. The changes due to the long irradiation are unexpectedly small. The rod wrapping wires are not appreciably loose and it appears that these rods will be suitable for reirradiation. Since they are in good condition, some may be used as drivers in the reirradiation of 3 to 7 of the F9C-1 rods from which the wires have been removed. This procedure would avoid going to the stacked grid subassembly but would severely limit the number of F9C-1 rods that could be included. The first F11A reirradiation has demonstrated the feasibility of certain combinations of wired and unwired rods in an irradiation vehicle.

The maximum diameter increases are listed in Table 3-4. These are from helical traces (since the rods still are wire wrapped) which are less precise than the 0° and 90° profiles for the F9C-1 series given in Table 3-3. The maximum diameter increase was less than 0.008 inch (0.2 mm) or about 3.1%. The diameter versus

* The system uses a matched pair of Linear Variable Differential Transformers (LVDT) wired to give a difference indication (as well as individual position); and the range of the instrument is affected by rod bowing, which was substantial. The out-of-range rod (F9C-24) will be remeasured, as well as rod F9C-1, which also is suspect.

TABLE 3-4 MAXIMUM DIAMETER CHANGES IN SERIES F9D-1 (X204) RODS

Rod	Maximum[a] Post Irradiation Diameter Inch	Diametral Increase		Peak	
		mils	%	Burnup %	Fast Fluence 10^{22}n/cm^2
F9D-4	.2567	5.8	2.3	13.2	6.63
F9D-5	.2552	4.8	1.9	13.0	6.50
F9D-7	.2579	7.1	2.8	13.4	6.79
F9D-8	.2569	6.0	2.4	13.2	6.65
F9D-9	.2551(.2558 spike)	4.7	1.9	13.0	6.52
F9D-11	.2582	7.2	2.9	13.6	6.96
F9D-12	.2571	6.6	2.6	13.4	6.81
F9D-13	.2566	6.2	2.5	13.2	6.67
F9D-14	.2552	4.5	1.8	13.0	6.53
F9D-16	.2574	7.1	2.8	13.6	6.98
F9D-17	.2574	6.6	2.6	13.4	6.83
F9D-18	.2561	5.3	2.1	13.2	6.68
F9D-20	.2580	7.5	3.0	13.6	6.98
F9D-21	.2571	6.5	2.6	13.4	6.83
F9D-28	.2577	7.2	2.9	13.6	6.93
F9D-29	.2564	5.7	2.3	13.3	6.76
F9D-31	.2582	7.7	3.1	13.8	7.13
F9D-33	.2583	7.7	3.1	13.8	7.14
F9D-37	.2585	7.3	2.9	13.8	7.10

a) Near peak flux position, helical format

fluence data are plotted in Figure 3-2 together with the F9C-1 series results. These preliminary data suggest that the incubation fluence for diameter increase in Type-316 annealed clad rods is about 4.5×10^{22} n/cm^2 with a rate of approximately 1.1% diameter increase per 10^{22} n/cm^2. This is fairly consistent with the length changes observed in X143A (Table 3-2).

3.1.4 F9E

The F9E (X145) grid spaced experiment completed its irradiation to a maximum-rod peak burnup of 11.7% (7.5×10^{22} n/cm^2 fast fluence) in Run 75. After an extended cooling period to allow for full subassembly neutron radiography, the irradiation vehicle was disassembled and the rods were examined at HFEF/N. Less than 3% diametral swelling was observed; all rods are intact and suitable for continued irradiation. The HFEF examinations were completed during this reporting period and eighteen rods were shipped to LASL for terminal examination. The remaining nineteen are awaiting only the availability of a shipment cask for transfer from HFEF to LASL.

The radiation-induced swelling of austenitic stainless steel normally results in maximum cladding diametral increases near the core mid-plane. Post-irradiation profilometry of the F9E subassembly rods showed the normal diametral increase near the core mid-plane, but in addition, significant secondary swelling peaks were observed for some rods near the top of the fuel column. All of the F9E rods are clad in annealed 316 stainless steel. Figure 3-2 shows the predicted* and measured* cladding profile for rods F9E-4 and F9E-23. As can be observed, rod F9E-4 shows a pronounced secondary swelling peak while rod F9E-23 shows a much less pronounced secondary swelling peak. The NSMH* correlation predicted the magnitude of the observed mid-core cladding quite accurately for the two rods but the observed temperature dependence is slightly discrepant. The mid-core cladding diametral changes observed for the F9E rods can, therefore, be attributed primarily to radiation-induced swelling of the cladding. The secondary peaks are not predicted by the NSMH correlation.

---

* The predictions used the Nuclear Systems Materials Handbook [3-2] (NSMH) correlations for annealed type 316; the measured values given in this report are average diameters at four equally spaced orientations around the circumference of the rod.

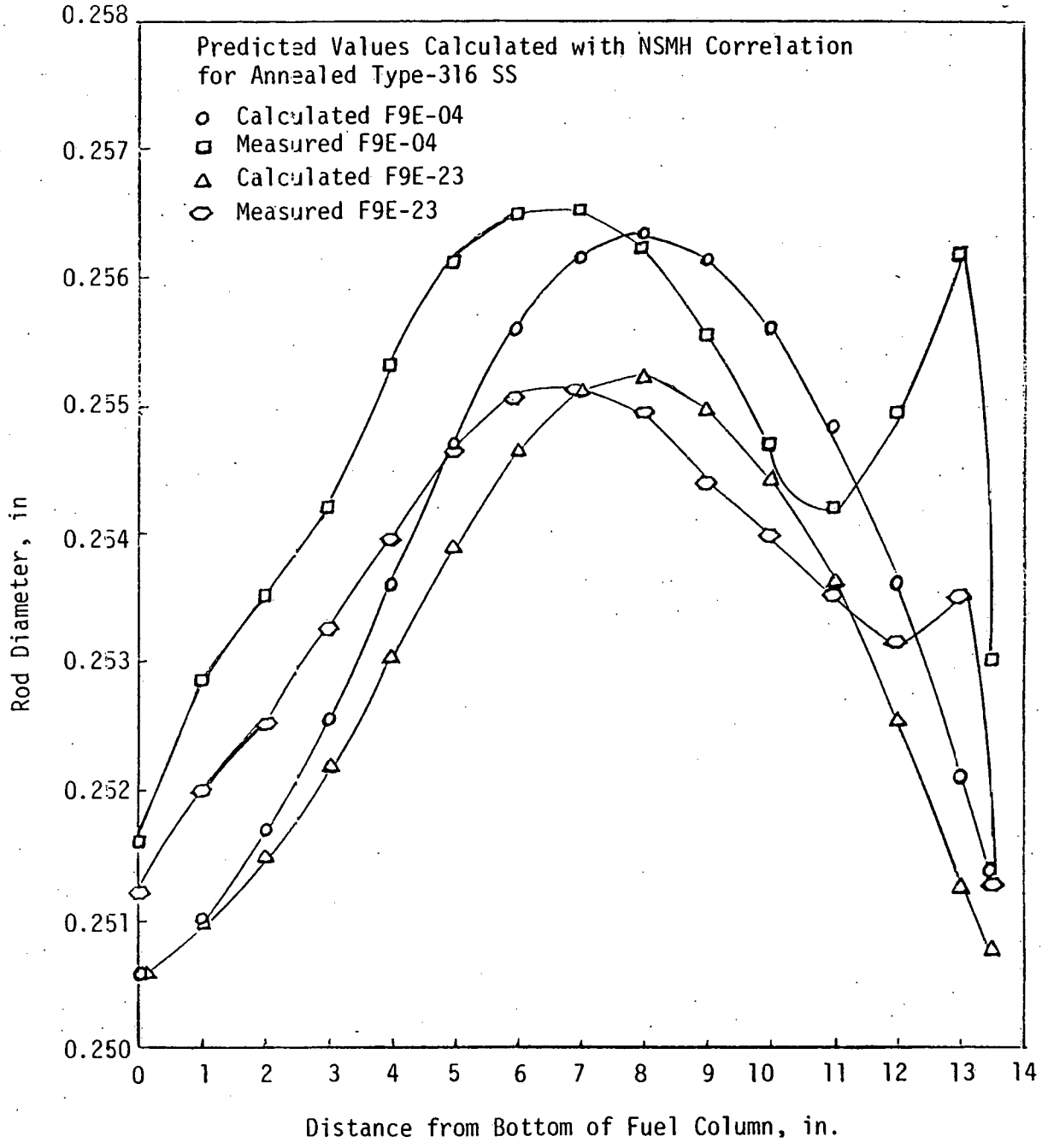

FIGURE 3-2. PREDICTED CLADDING PROFILES DUE TO IRRADIATION-INDUCED SWELLING VERSUS MEASURED PROFILES FOR FUEL RODS F9E-04 AND F9E-23.

Figure 3-3 shows the observed variations in rod diameter increase across the F9E subassembly (from highest to lowest fission rate positions), and Figure 3-4 shows the locations of the same rods within the subassembly. Table 3-4 shows the accumulated cladding fluences and life average mid-wall cladding temperatures at selected axial planes along the rods. As can be observed from Figure 3-3, rods F9E-1 and F9E-27, which are adjacent to the channel wall*, do not show a secondary swelling peak, although the rods do show more pronounced cladding diametral change at the top of the fuel column than would be predicted due to normal cladding swelling. Growth of the secondary peak in the interior rods appears to be a very sensitive function of temperature and fluence (see Table 3-5). The mechanism causing growth of this secondary peak is presently not established and the analysis is continuing.

3.2 LOW POWER IRRADIATIONS

3.2.1 F8B

3.2.1.1 Irradiation

Nineteen encapsulated F8B rods were irradiated in X036, beginning with run 29D and ending in run 45 at approximately 4% peak burnup. After an interim examination at HFEF, the rods were reconstituted into two MK-A19 subassemblies: X117 (9 rods) and X118 (10 rods) that were irradiated beginning in run 47 and ending in run 55, achieving 5-6% burnup. Throughout these early irradiations, the subassemblies were located in the outer regions of row 7 or inner positions in row 8, so that peak linear power was below 7 kW/ft, with the exception of the initial exposure in run 29D to approximately 0.25% burnup at 7-1/2 to 9-1/2 kW/ft peak. The insertion of the second EBR-II radial reflector, beginning in run 56, increased the axial peak fission rates at the periphery of the core and flattened the axial profile. Because of concern that substantial power increases in low power rods would lead to cladding breach**, it was decided to perform a second set of interim

---

* Therefore, they have substantially cooler cladding.

** In fact, both of the low power FO series rods in run 56 (XG04B) did breach in run 56; (XG04B was inserted only in run 56).

TABLE 3-5

ACCUMULATED CLADDING FLUENCE AND LIFE AVERAGE MID-WALL CLADDING TEMPERATURE FOR SELECTED RODS FROM F9E SUBASSEMBLY

DISTANCE FROM BOTTOM OF FUEL COLUMN, IN.	F9E-01 HIGHEST RATE	F9E-04	F9E-41	F9E-42	F9E-17	F9E-23	F9E27 LOWEST RATE
			LIFE AVE. MID-WALL CLADDING TEMPERATURE, °F				
0	778	771	771	769	769	767	772
1	793	788	788	786	785	783	786
2	812	808	808	805	806	803	803
3	831	830	830	827	827	823	822
4	852	852	853	848	848	844	841
5	872	874	874	870	870	864	859
6	891	895	896	892	890	885	877
7	910	916	917	912	911	905	894
8	927	936	937	932	930	923	912
9	945	955	956	950	949	941	927
10	960	973	974	969	966	958	941
11	975	990	991	985	983	974	956
12	989	1005	1007	1001	998	989	968
13	1004	1022	1025	1018	1016	1005	982
13.5	1013	1032	1034	1028	1025	1014	992
			END-OF-IRRADIATION CLADDING FLUENCE $X10^{-22}$, $^{n}/cm^{2}$				
0	4.61	4.50	4.45	4.33	4.28	4.14	4.08
1	5.51	5.38	5.32	5.18	5.11	4.95	4.87
2	6.21	6.06	6.00	5.83	5.76	5.57	5.49
3	6.72	6.56	6.49	6.31	6.23	6.03	5.94
4	7.09	6.92	6.85	6.66	6.57	6.36	6.27
5	7.33	7.15	7.08	6.88	6.79	6.58	6.48
6	7.44	7.26	7.18	6.98	6.90	6.68	6.58
7	7.43	7.25	7.18	6.97	6.89	6.67	6.57
8	7.32	7.14	7.06	6.87	6.78	6.57	6.47
9	7.11	6.93	6.86	6.67	6.59	6.38	6.28
10	6.81	6.64	6.57	6.39	6.31	6.11	6.02
11	6.39	6.23	6.17	6.00	5.92	5.73	5.65
12	5.80	5.65	5.60	5.44	5.37	5.20	5.12
13	4.99	4.87	4.82	4.68	4.63	4.48	4.41
13.5	4.55	4.41	4.34	4.23	4.20	4.07	3.98

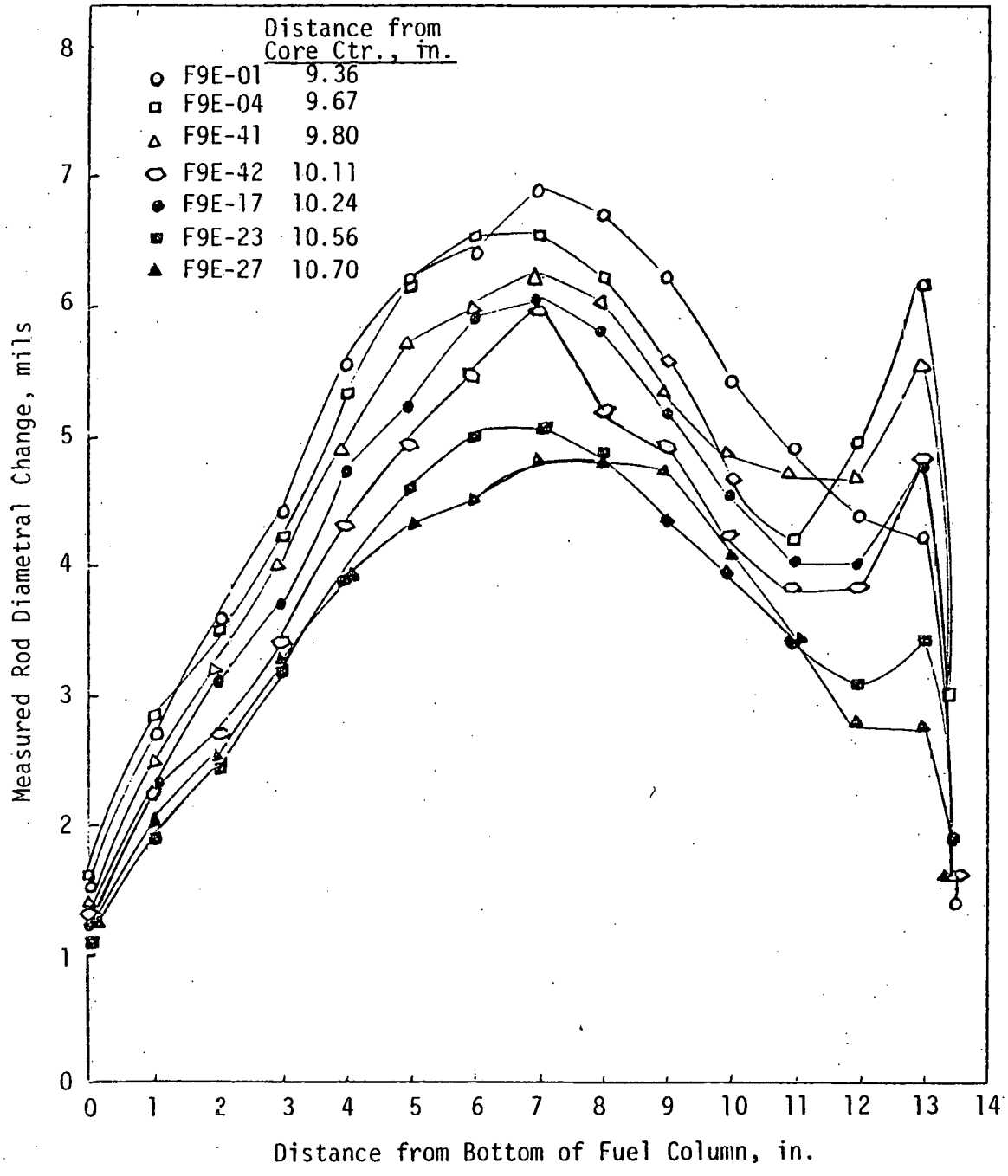

FIGURE 3-3. OBSERVED VARIATION IN ROD DIAMETRAL CHANGE ACROSS F9E SUBASSEMBLY.

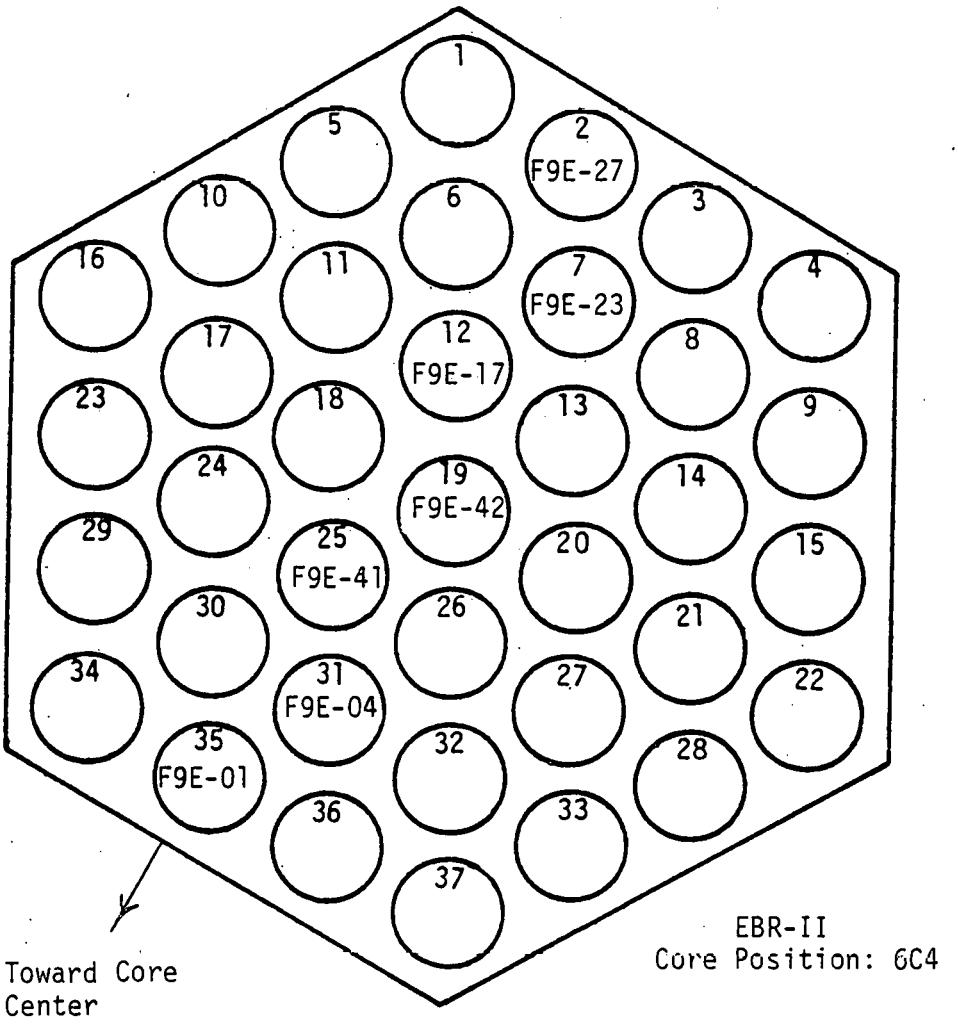

FIGURE 3-4. SUBASSEMBLY POSITION OF F9E (X145) RODS OF FIGURE 3-3.

examinations at the end of run 55 to establish pre-reflector conditions. It was shown that no rods were breached after run 55. The nine X117 rods were reconstituted in X117A, which was exposed in run 58 only, at location 9C8 where peak power was 8.2 to 9.4 kW/ft.

Table 3-6 shows the major power changes for this experiment, together with the final burnup and fast fluence values. The peak powers at the beginning of X117A were more than double the corresponding power in X117 (increases ranged from 105% to 127%). Local power will have been increased again by 10-20% at the ends of the rods. The X117A rods received a third interim examination after run 58 and no cladding breaches were detected. Three rods each from X118 and X117 were then shipped to LASL for destructive examination. The remaining X117A rods were reconstituted into X117B (6 rods), and the X118 rods formed X118A (7 rods) (with the exception that one X117A rod was inserted in X118A and one X118 rod was included in X117B). X118A was irradiated at location 9C1 at about five kW/ft, which was fairly similar to the X117 and X118 power before the reflector was installed (-21% to -2% in the X118 rods and +33% in the single X117, X117A rod). Subassembly X117B was inserted somewhat closer to the core centerline at 9C8 and produced 6-7 kW/ft peak, intermediate between the run 55 power (X117) before the reflector and the run 58 power (X117A) with the reflector (+52% to +73% in X117B versus X117 compared to +10% to +127% in X117A, and +8% in the single X117B rod that was in X118). Table 3-7 presents the power and burnup history of the F8B series rods and these major changes are plotted in Figures 3-5 (X117A) and 3-6 (non X117A). The X117B and X118A irradiations began in run 63 and ended with runs 77A and 78C respectively, acheiving 9.6% to 11.1% peak burnup at 2.5 to 3.7 cm^{-2} peak fast fluence. Because the series began irradiation in a comparatively hard neutron spectrum and ended in the substantially softer reflector zone, and rods were removed at two burnup levels, there is a substantial variation of fluence-to-burnup ratio in the F8B rods (0.26 to 0.47 x 10^{22} n/cm^2 per percent burnup.

The final examination of the X117B and X118A rods at HFEF produced no evidence of cladding breach in any F8B series rod. It is difficult to reconcile the complete absence of cladding breach in the F8B series with the total breach in the overpowered F0 series (XG04B), on the basis of irradiation history. The

TABLE 3-6

POWER CHANGES, PEAK BURNUP AND FLUENCE IN F8B SERIES RODS

ROD	END OF RUN 55 [a] PEAK POWER KW/FT	START OF RUN 58[b] PEAK POWER KW/FT	PERCENT DIFFERENCE RUN 58 VS. RUN 55	START OF RUN 63[c] PEAK POWER KW/FT	DIFFERENCE RUN 63 VS. RUN 55	FINAL SUBASSEMBLY [i]	FINAL PEAK BURNUP %	TOTAL PEAK FAST FLUENCE $10^{22}n/cm^2$	$\left(\frac{\text{FLUENCE}}{\text{BURNUP}}\right)$ RATIO
F8B-1	5.69	[d]	-	5.37	-5.6	X118A	9.59	2.49	.260
2	5.77	[d]	-	4.71	-18.4	X118A	11.00	3.66	.333
3	3.78	8.59	127.2	[g]	-	X117A	6.06	2.50	.413
4	4.55	9.33	105.1	6.94	+52.5	X117B	10.86	3.63	.334
5	5.54	[e]	-	-	-	X118	5.11	1.89	.370
6	5.45	[d]	-	5.30	-2.8	X118A	9.59	2.47	.258
7	4.49	9.38	108.9	[g]	-	X117A	5.73	2.18	.380
8	6.12	[d]	-	4.85	-20.8	X118A	11.12	3.69	.332
9	6.04	[e]	-	-	-	X118	6.63	3.09	.466
10	4.26	9.15	114.8	6.81	+59.8	X117B	10.83	3.52	.325
11	3.68	8.20	122.8	6.15	+67.1	X117B	10.82	3.48	.322
12	5.69	[e]	-	-	-	X118	6.20	2.70	.435
13	5.56	[f]	-	6.02	+8.3	(X117B)[i]	10.58	3.36	.318
14	4.08	9.07	122.3	6.78	+66.2	X117B	10.56	3.34	.316
15	3.57	8.28	131.9	6.16	+72.5	X117B	10.82	3.50	.323
16	4.22	8.91	111.1	[g]	-	X117A	5.92	2.33	.394
17	4.12	9.05	119.7	5.48[h]	+33.0	(X118A)[i]	10.32	2.95	.286
18	5.64	[d]	-	5.35	-5.1	X118A	10.51	3.26	.310
F8B-19	5.81	[d]	-	5.34	-8.1	X118A	10.58	3.31	.313

a) In X117 or X118
b) In X117A
c) In X117B or X118A
d) In X118A, not in X117A
e) PIE after run 55 (X118)
f) From X118 to X11TB
g) Pie after run 58 (X117A)
h) From X117A to X118A
i) Parenthesis indicates interchange between X117 series and X118 series.

TABLE 3-7 SERIES F8B HISTORY

Rod	Start X036 Run29D Power	X036 Start Run30 Power	X036 Start Run30 Burnup	End X036 Run45 Burnup	Start X117 Run47 Power	End X117 Run55 Power	End X117 Run55 Burnup	Start X118 Run47 Power	End X118 Run55 Burnup	Start X117A Run58 Power	End X117A Run58 Burnup	Start X117B Run63 Power	End X117B Run77A Power	End X117B Run77A Burnup	Start X118A Run63 Power	End X118A Run78C Burnup
F8B-1	7.71	5.28	0.20	3.41	-	-	-	6.04	5.10	-	-	-	-	-	5.37	9.59
" -2	9.03	6.52	0.26	4.67	-	-	-	6.15	6.59	-	-	-	-	-	4.71	11.00
" -3	9.35	6.59	0.25	4.35	4.79	3.78	5.71	-	-	8.59	6.06	-	-	-	-	-
" -4	8.14	5.57	0.22	3.72	5.79	4.55	5.35	-	-	9.33	5.74	6.94	7.92	10.86	-	-
" -5	7.60	5.20	0.20	3.43	-	-	-	5.87	5.11	-	-	-	-	-	-	-
" -6	7.59	5.19	0.20	3.43	-	-	-	5.79	5.08	-	-	-	-	-	5.30	9.59
" -7	8.19	5.60	0.22	3.73	5.71	4.49	5.34	-	-	9.38	5.73	-	-	-	-	-
" -8	9.32	6.73	0.26	4.70	-	-	-	6.52	6.69	-	-	-	-	-	4.85	11.12
" -9	9.33	6.74	0.26	4.68	-	--	-	6.44	6.63	-	-	-	-	-	-	-
" -10	8.91	6.16	0.23	4.02	5.41	4.26	5.52	-	-	9.15	5.89	6.81	7.79	10.83	-	-
" -11	8.97	6.32	0.25	4.35	4.66	3.68	5.73	-	-	8.20	6.08	6.15	7.05	10.82	-	-
" -12	8.85	6.23	0.25	4.36	-	-	-	6.05	6.20	-	-	-			-	-
" -13	8.31	5.74	0.23	4.05	-	-	-	5.91	5.85	-	-	6.02	6.91	10.58	-	-
" -14	8.19	5.60	0.22	3.73	5.17	4.08	5.19	-	-	9.07	5.56	6.78	7.75	10.56	-	-
" -15	8.96	6.31	0.25	4.37	4.52	3.57	5.70	-	-	8.28	6.06	6.16	7.06	10.82	-	-
" -16	8.77	6.07	0.23	4.04	5.36	4.22	5.55	-	-	8.91	5.92	-	-	-	-	-
" -17	8.11	5.55	0.22	3.72	5.23	4.12	5.21	-	-	9.05	5.58	-	-	-	5.48	10.32
" -18	8.53	5.89	0.23	4.02	-	-	-	5.99	5.79	-	-	-	-	-	5.35	10.51
" -19	8.58	5.93	0.23	4.04	-	-	-	6.18	5.87	-	-	-	-	-	5.34	10.58

(a) Peak Power in kW/ft, Peak Burnup in percent.

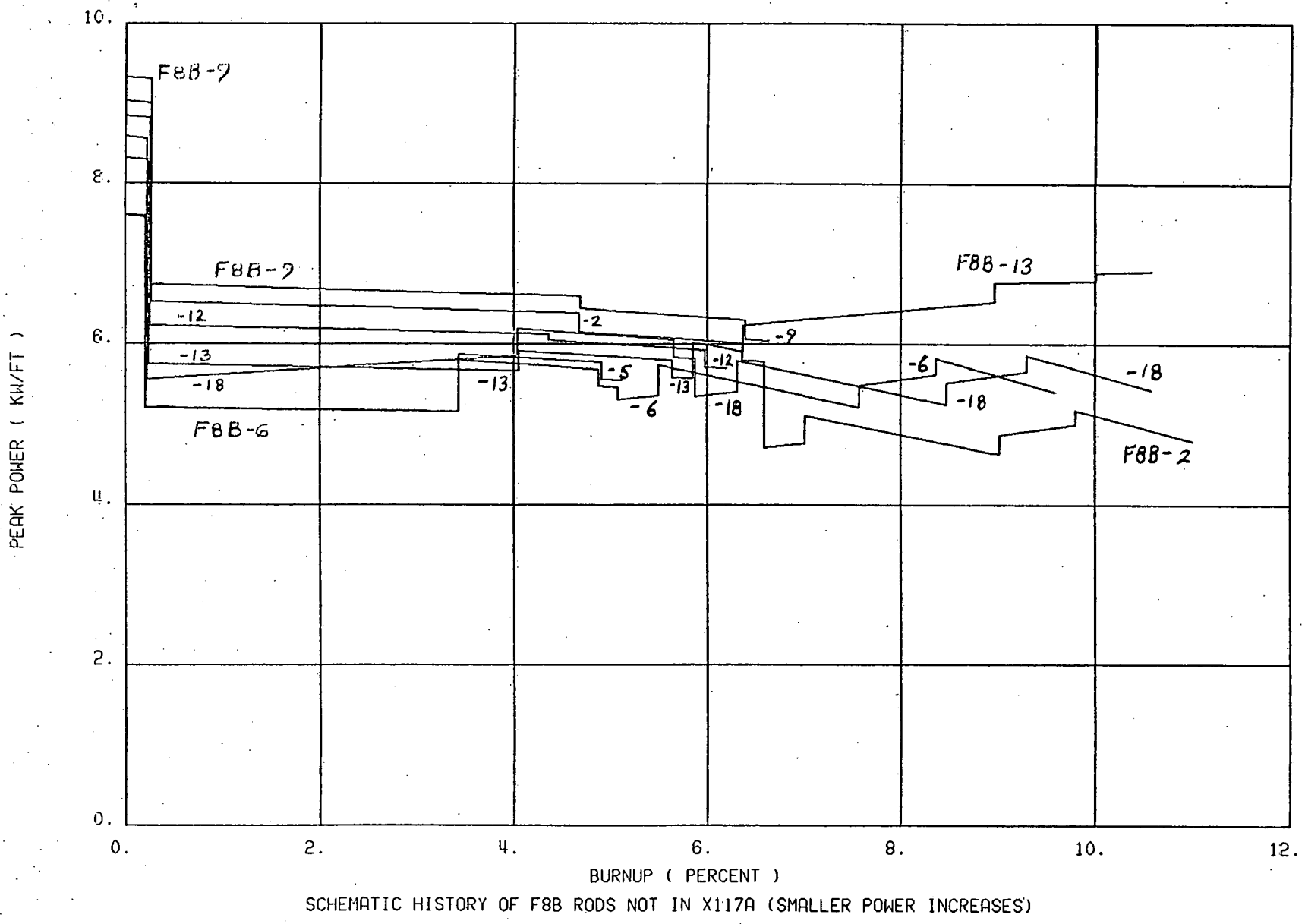

SCHEMATIC HISTORY OF F8B RODS NOT IN X117A (SMALLER POWER INCREASES)

FIGURE 3-5

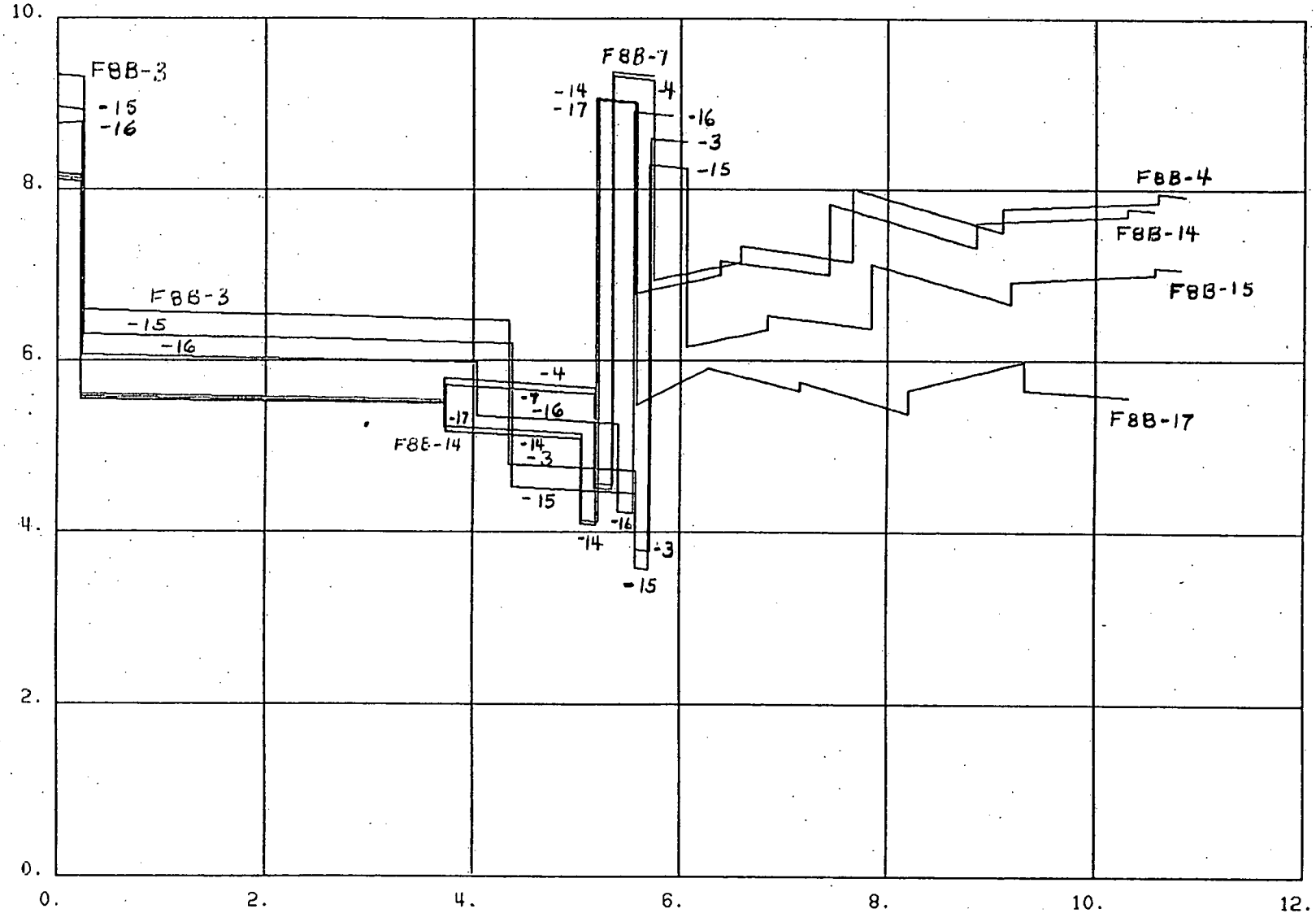

SCHEMATIC HISTORY OF F8B RODS IN X117A (LARGE POWER INCREASE AT RUN 58)

FIGURE 3-6

relative increase in F8B between end of run 55 and start of run 56 was equivalent to or greater than the same for FO*. Both sets had an early life higher power period at 8 to 9-1/2 kW/ft, but this occurred in the initial 0.25% burnup for F8B and at 2-4% burnup in FO. Also, the run 56 overpower occurred later in life in FO (9-10% burnup) than in F8B (5-6% burnup). Probably of more importance than the historical irradiation paths, however, are the major differences in fuel rod parameters. The FO rods that breached in XGO4B had fuel cladding gaps as low as 1.1 mils, high O/M (1.998-1.999), high smeared density (92-93%), and they were clad in annealed 347. The F8B rods that survived X117A had larger gaps (2.5 mils minimum, typically 5 mils), lower smeared density (84-88%), generally lower O/M (1.95-1.98 except for one rod at 2.016) and they were clad in annealed 304, 316 or I-800. The F8B rods also contained solid, dished, or annular pellet fuels or vibratorily comparted powder, but the FO fuels were in the form of solid pellets. The small fuel-cladding gap is probably of prime importance in the FO cladding breaches[3-1], so that the larger as-fabricated gaps in F8B constituted a major factor in their survival in X117A.

The X117B and X118A rods were shipped to LASL for post-irradiation evaluation. The non-destructive examinations are nearly complete. Specifications are being established for the destructive examination of selected F8B series rods, but the testing is not expected to be performed for at least a year because of higher priority work.

3.2.1.2 Post-Irradiation Examination of Six X118 and X117A Rods

The F8B experiment consists of 19 encapsulated fuel rods containing fully enriched mixed oxide fuels with Pu contents of 25% Pu/(U+Pu). Fuel configurations include solid pellets, annular pellets, dished-end pellets and Vipac powder. Pellet densities were 87-97%, and smeared densities ranged from 81-92%. The claddings were annealed Types-304 and -316 stainless steel, 20% cold-worked Type-304 stainless steel and annealed Incoloy-800. The nominal cladding diameter is 0.25-inch (6 mm) with wall thickness of 0.015-inch (0.4 mm). Local fuel cladding diametral gaps ranged from 2.5-9.3 mils (60-240 μm). Rod mean gaps were 3.3 to 8.1 mils (80-210 μm). Table 3-8

---

* End of run 55 peak powers were 4.8 and 5.6 kw/ft in XGO4A and 5.2 and 5.7 kw/ft in X117. At start of run 56 the values were 8.6 and 10.0 in XGO4B but 8.2 to 9.4 kw/ft in X117A.

TABLE 3-8

FUEL FABRICATION PARAMETERS

FUEL ROD	CLADDING TYPE	FUEL TYPE[d]	FUEL DENSITY, % PELLET	FUEL DENSITY, % SMEARED	O/M	FUEL-CLADDING DIAMETRAL GAP, mils RANGE	FUEL-CLADDING DIAMETRAL GAP, mils MEAN	In X117A ?
A. RODS IRRADIATED UP TO ~6% BURNUP (X036, X117, X117A, X118)								
F8B-3	I800	SP	94.88	88.05	1.972	7.2-9.0	8.1	Yes
F8B-5	304[a b]	SP	94.33	90.49	1.974	3.0-5.8	4.5	No
F8B-7	I800	DP	95.34	87.96	1.976	3.6-6.4	5.1	Yes
F8B-9	316	SP	85.98	83.40	1.972	2.4-4.4	3.3	No
F8B-12	I800	VC	-	83.20	1.977	-	-	No
F8B-16	304[a]	AP	96.36	87.43	1.971	4.1-6.3	5.2	Yes
B. RODS IRRADIATED UP TO ~ 11% BURNUP (A. plus X117B, X118A)								
F8B-1	304[a,b]	SP	94.86	92.16	1.976	2.5-3.9	3.1	No
F8B-2	316	SP	83.63	80.82	1.973	3.0-4.4	3.7	No
F8B-4	316	AP	96.40	87.62	1.974	4.3-5.8	5.1	Yes
F8B-6	316	DP	95.89	88.40	1.958	4.7-6.1	5.2	No
F8B-8	316	VC	-	83.04	1.977	-	-	No
F8B-10	316	SP[c]	92.98	89.57	2.016	3.5-5.0	4.1	Yes
F8B-11	I800	SP	87.32	84.49	1.955	2.5-5.2	3.6	Yes
F8B-13	304	VC	-	83.00	1.976	-	-	No
F8B-14	304	DP	95.74	87.80	1.978	3.6-6.2	5.8	Yes
F8B-15	316	DP	90.64	83.80	1.977	4.1-6.2	5.2	Yes
F8B-17	316	AP	96.59	87.25	1.969	3.0-9.3	6.1	Yes
F8B-18	316	AP	95.63	84.95	1.973	4.5-6.1	5.2	No
F8B-19	316	SP	90.59	85.52	1.972	2.6-9.3	6.2	No

*a) These claddings are seamless, the rest are weld-drawn.
b) These claddings are 20% Cold Worked the rest are annealed and ballized.
c) This fuel was mechanically mixed, the rest were coprecipitated.
d) SP = solid pellet, AP - annular pellet,
DP = dished pellet, VC - vibrationally compacted powder.

summarizes the fuel fabrication parameters. These rods operated at linear powers ranging from 5 to 10 kW/ft (16 to 33 kW/m). Burnup in excess of 11% was achieved. The irradiation vehicles and exposures were described in the preceding section.

Nondestructive examinations showed that no cladding breaches have occurred in the F8B series rods. Post-irradiation examinations of the nominally 6% burnup rods are described here. Of these six rods, three were from X117A (F8B-3, -7, -16) where an 8 to 9-1/2 kW/ft (26-31 kW/m, 105-127%) overpower condition prevailed during run 58. The remaining three were taken from X118 at the end of run 55, and they (F8B-5, -9, -12) did not receive this overpower irradiation. Figures 3-7 and 3-8 show the peak linear power and cladding maximum temperature histories of these rods. Tables 3-9 and 3-10 describe the calculated local irradiation conditions for the destructively examined samples. Results of the examinations performed at Los Alamos Scientific Laboratory are described in the following paragraphs.

a. Radiography

Betatron radiographs of the encapsulated rods showed all six rods to be in good condition. There was no evidence of cladding breach or irradiation-induced central void formation in any rod. The pellet-to-pellet interfaces in the solid pellet rods (F8B-3, -5, -9, -16) were visible. In F8B-3, there was a ~0.8 mm (.03 in) separation between the eighth and ninth pellets from the bottom. The dished-end shapes of all of the F8B-7 pellets were still evident. The annular pellets in F9B-16 showed no irregularities. Four Ta spacers used to separate the enriched and depleted UO_2 pellets in the blanket region (natural UO_2) were clearly identifiable in each of the pellet rods (F8B-3, -5, -7, -9, -16).

b. Gamma Scans

Gross and isotopic gamma scans were made for the encapsulated rods. The gross scans were similar, one to another, except for vibratorilly compacted rod F8B-12. All pellet fuel showed activity spikes approximately 2.5 inches (64 mm) above the fuel column. These corresponded to the enriched UO_2 pellet and the Ta spacers in the blanket region. The fuel columns showed relatively smooth activity distributions in all five rods with an approximate cosine curve profile. Slightly higher activity was detected at the top end of the fuel column in F8B-3 and F8B-9, while F8B-16 showed slightly

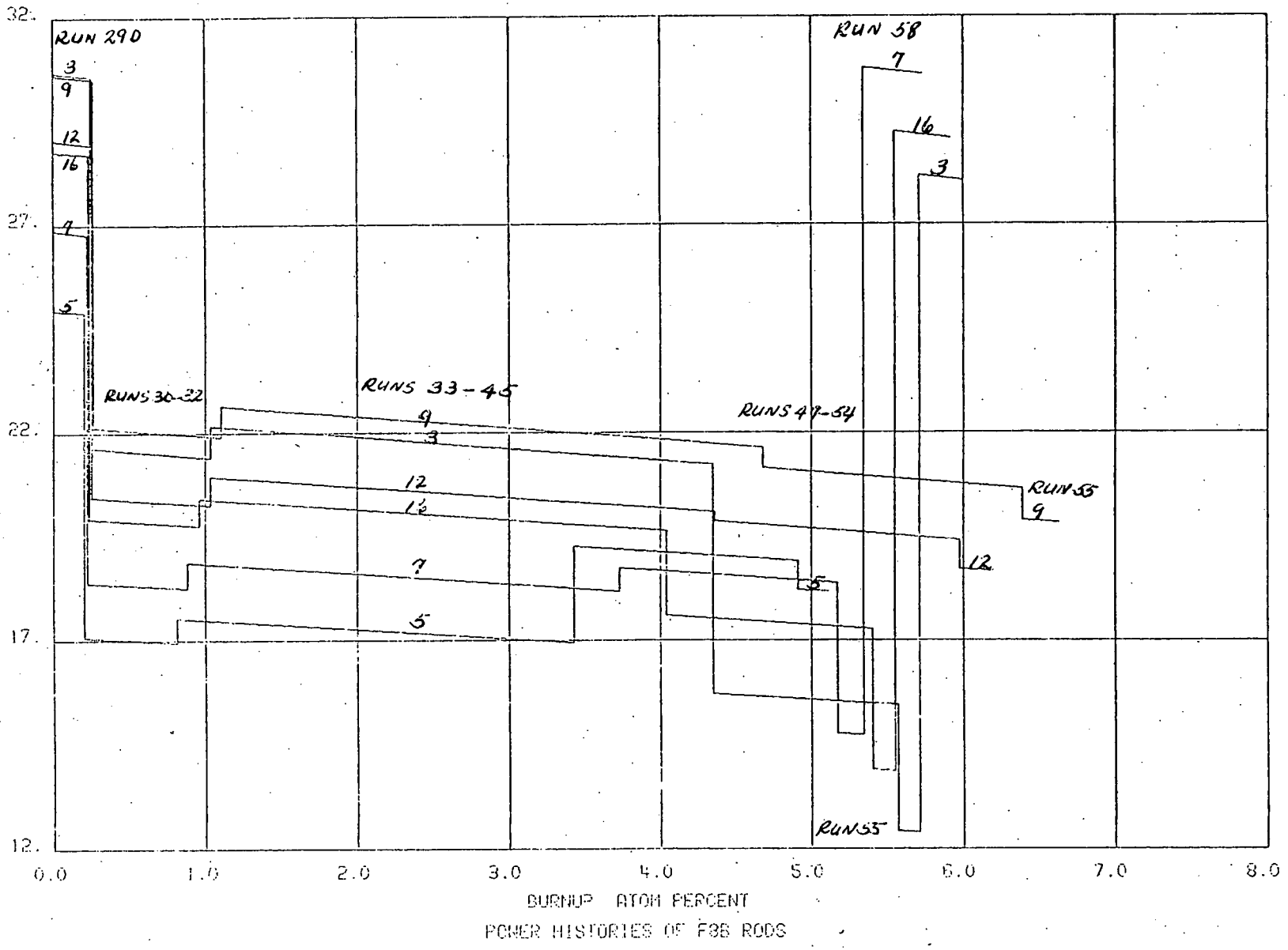

POWER HISTORIES OF F3S RODS

FIGURE 3-7

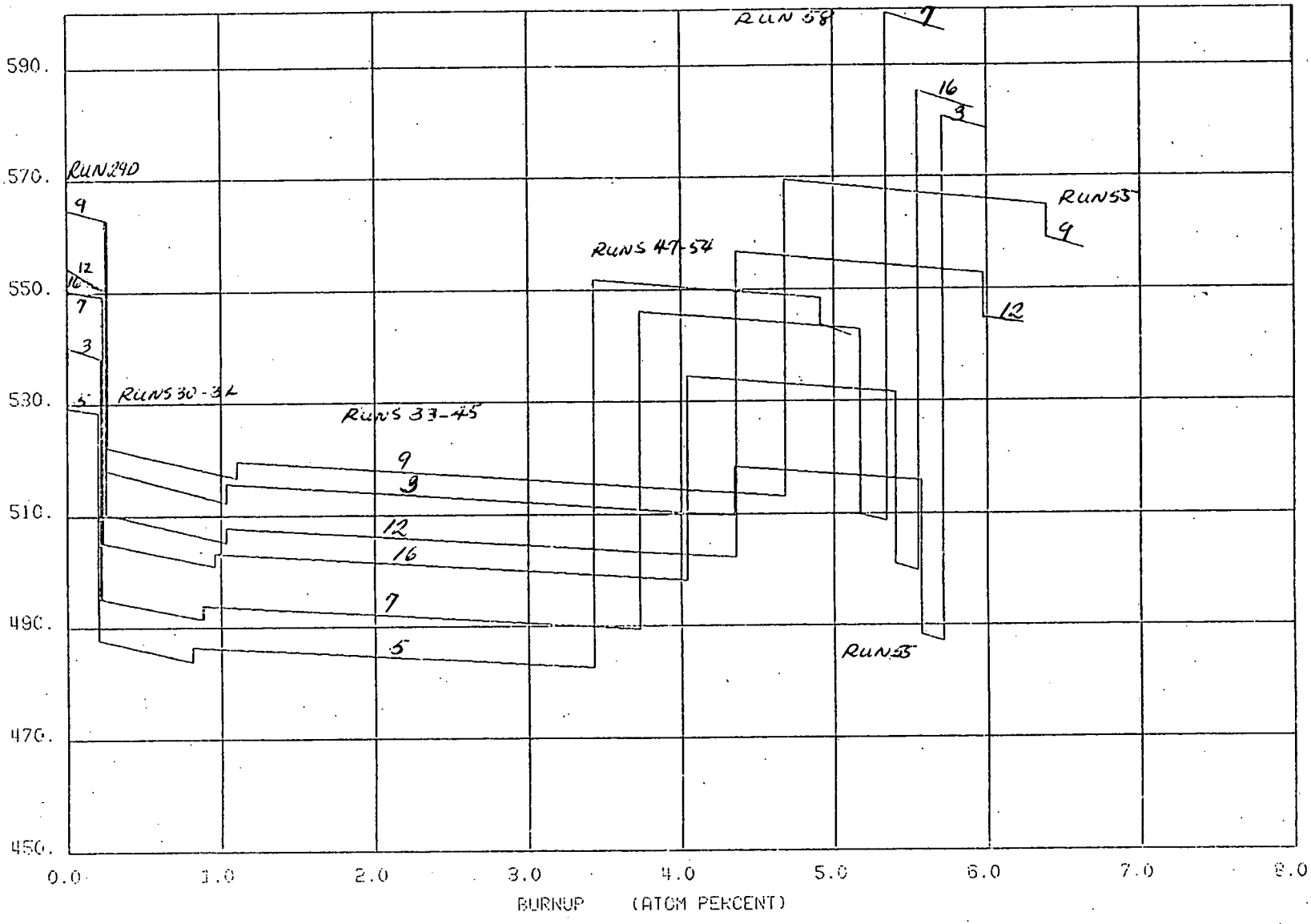

MAXIMUM CLADDING TEMPERATURE HISTORIES

FIGURE 3-8

TABLE 3-9

LOCAL IRRADIATION CONDITIONS CALCULATED FOR THE TESTED SAMPLES
IN THE 6% BURNUP F8B RODS PRIOR TO RUN 55

FUEL ROD	SEC-TION	SECTION TYPE	AXIAL[a] DISTANCE (mm)	END OF RUN 45 BURNUP (%)	END OF RUN 45 FAST FLUENCE ($^n/cm^2 X 10^{22}$)	BEGINNING OF LIFE (RUN 29D) LINEAR POWER (Kw/m)	BEGINNING OF LIFE (RUN 29D) TEMPERATURE, °C CLAD O.D.	BEGINNING OF LIFE (RUN 29D) TEMPERATURE, °C CLAD I.D.	POST RUN 45*[b] LINEAR POWER (Kw/m)	POST RUN 45*[b] TEMPERATURE, °C CLAD O.D.	POST RUN 45*[b] TEMPERATURE, °C CLAD I.D.
F8B-3	C	BURNUP	138	4.35	2.01	30.6	490	520	21.2	453	475
	D	TRANS MICRO	154	4.35	2.01	30.7	497	527	21.3	458	480
	E	CLAD DENSITY	166	4.33	2.00	30.6	502	532	21.2	462	483
	G	BURNUP	308	3.39	1.56	24.4	546	569	16.9	492	509
	H	CLAD DENSITY	321	3.28	1.51	23.8	549	571	16.5	494	510
	I	LONG MICRO	345	3.08	1.42	22.7	555	576	15.7	498	513
F8B-5	C	BURNUP	126	3.39	1.29	24.7	463	489	16.8	433	452
	D	TRANS MICRO	142	3.43	1.30	24.9	469	495	17.0	438	456
	E	CLAD DENSITY	147	3.43	1.30	24.9	471	497	17.0	439	470
	H	CLAD DENSITY	319	2.66	1.01	19.4	514	534	13.2	468	482
	I	LONG MICRO	342	2.56	0.97	18.5	519	538	12.6	471	485
F8B-7	B1	LONG MICRO	111	3.66	1.48	26.3	464	490	17.8	434	452
	C	BUNRUP	130	3.72	1.50	26.7	472	499	18.1	439	458
	D	TRANS MICRO	146	3.73	1.51	26.9	478	505	18.2	444	462
	E	CLAD DENSITY	149	3.73	1.51	26.9	479	506	18.2	445	463
	H	CLAD DENSITY	303	2.93	1.18	21.6	523	544	14.7	474	488
	I	LONG MICRO	336	2.80	1.13	20.2	529	549	13.7	478	492
F8B-9	B	LONG MICRO	8	3.72	1.82	24.5	425	450	17.3	409	427
	C	CLAD DENSITY	21	3.93	1.93	25.3	431	457	18.5	414	432
	E	BURNUP	138	4.67	2.29	30.5	489	518	21.6	454	476
	F	TRANS MICRO	153	4.68	2.29	30.6	496	525	21.7	459	481
	G	CLAD DENSITY	166	4.67	2.29	30.5	501	530	21.6	463	484
	I	BURNUP	301	3.74	1.83	24.7	540	566	17.5	493	509
	J	CLAD DENSITY	305	3.63	1.78	24.5	544	567	17.4	493	510
	K	LONG MICRO	339	3.51	1.72	22.8	550	573	16.2	499	514
F8B-12	C	BURNUP	138	4.35	1.99	28.9	483	509	20.1	449	467
	D	TRANS MICRO	153	4.36	1.99	29.0	490	516	20.1	453	472
	E	CLAD DENSITY	166	4.35	1.99	28.9	494	520	20.1	457	475
	H	CLAD DENSITY	318	3.38	1.55	22.6	538	558	15.7	487	501
	I	LONG MICRO	340	3.26	1.49	21.6	543	562	15.0	490	503
F8B-16	C	BURNUP	127	4.00	1.72	28.5	477	504	19.5	444	462
	D	TRANS MICRO	143	4.04	1.74	28.7	484	511	19.7	448	467
	E	CLAD DENSITY	147	4.04	1.74	28.8	486	513	19.7	450	468
	H	CLAD DENSITY	319	3.13	1.35	22.4	537	557	15.3	484	498
	I	LONG MICRO	342	3.01	1.29	21.6	542	561	14.6	487	501

a) Bottom of core to midpoint of specimen except bottom of core to top of specimen (surface polished) for trans micro.
b) These rods were irradiated in subassembly X036, location 7E1 up to run 45 after which the rods were reconstituted into subassemblies X117 and X118.

TABLE 3-10

LOCAL IRRADIATION CONDITIONS CALCULATED FOR THE TESTED SAMPLES

IN THE 6% BURNUP F8B RODS AT END OF LIFE ((RUNS 55 and 58)

FUEL ROD	SECTION	SECTION TYPE	AXIAL DISTANCE (mm)	END OF LIFE BURNUP (%)	END OF LIFE FAST FLUENCE (10^{22}n/cm^2)	POST RUN 55* LINEAR POWER (Kw/m)	POST RUN 55* TEMPERATURE, °C CLAD O.D.	POST RUN 55* TEMPERATURE, °C CLAD I.D.	END OF RUN 58 LINEAR POWER (Kw/m)	END OF RUN 58 TEMPERATURE, °C CLAD O.D.	END OF RUN 58 TEMPERATURE, °C CLAD I.D.
F8B-3	C	BURNUP	138	6.03	2.48	12.4	433	445	28.0	483	511
	D	TRANS MICRO	154	6.05	2.49	12.4	437	450	28.1	490	517
	E	CLAD DENSITY	166	6.05	2.49	12.4	440	453	28.1	494	522
	G	BURNUP	308	5.88	2.42	10.7	474	485	27.3	548	574
	H	CLAD DENSITY	321	5.85	2.41	10.5	476	487	27.3	553	579
	I	LONG MICRO	345	5.85	2.41	10.0	481	491	27.2	563	588
F8B-5	C	BURNUP	126	5.04	1.86	17.9	456	475	* -	-	-
	D	TRANS MICRO	142	5.09	1.88	18.1	462	482	-	-	-
	E	CLAD DENSITY	147	5.10	1.89	18.1	464	484	-	-	-
	H	CLAD DENSITY	319	4.29	1.59	15.4	525	540	-	-	-
	I	LONG MICRO	342	4.13	1.53	14.7	531	546	-	-	-
F8B-7	B1	LONG MICRO	111	5.66	2.15	14.4	435	450	30.4	481	512
	C	BURNUP	130	5.69	2.16	14.6	441	456	30.5	490	520
	D	TRANS MICRO	146	5.71	2.17	14.7	447	462	30.6	497	527
	E	CLAD DENSITY	149	5.72	2.17	14.7	448	463	30.6	498	528
	H	CLAD DENSITY	303	5.55	2.11	12.9	492	505	29.8	563	590
	I	LONG MICRO	336	5.54	2.10	12.1	500	512	29.8	576	604
F8B-9	B	LONG MICRO	8	5.49	2.56	16.5	410	427	* -	-	-
	C	CLAD DENSITY	21	5.70	2.66	16.8	415	432	-	-	-
	E	BURNUP	138	6.58	3.06	19.7	469	488	-	-	-
	F	TRANS MICRO	153	6.62	3.08	19.8	476	495	-	-	-
	G	CLAD DENSITY	166	6.63	3.09	19.9	426	501	-	-	-
	I	BURNUP	301	5.78	2.69	17.4	533	550	-	-	-
	J	CLAD DENSITY	305	5.60	2.61	17.2	535	551	-	-	-
	K	LONG MICRO	339	5.37	2.50	16.2	545	560	-	-	-
F8B-12	C	BURNUP	138	6.15	2.68	18.5	463	480	* -	-	-
	D	TRANS MICRO	153	6.19	2.70	18.7	470	487	-	-	-
	E	CLAD DENSITY	166	6.20	2.70	18.7	475	492	-	-	-
	H	CLAD DENSITY	318	5.21	2.27	15.8	529	543	-	-	-
	I	LONG MICRO	340	5.01	2.18	15.2	535	548	-	-	-
F8B-16	C	BURNUP	127	5.54	2.31	13.7	436	449	28.9	482	509
	D	TRANS MICRO	143	5.56	2.32	13.8	441	454	29.0	489	516
	E	CLAD DENSITY	147	5.57	2.33	13.8	443	456	29.1	491	518
	H	CLAD DENSITY	319	5.41	2.26	11.7	488	499	28.3	559	556
	I	LONG MICRO	342	5.39	2.25	11.2	493	503	28.2	568	593

*Run 55 was the End of Life Run for Rods F3B-5, -9 and -12.

greater activity at the bottom. This may indicate some fission product migration, but no multispectral scans were made over the fueled regions of these rods to identify the mobile species.

An activity spike was detected at approximately 0.76 in (19 mm) below each fuel column in the pellet rods, i.e., at the insulator/end plug interface. A short multispectral scan of F8B-16 over this region showed significantly more Zr-95/Nb-95 activity at this position than in the insulator, indicating the probability that small fragments of fuel had collected on the stainless steel bottom end plug during fabrication or irradiation. Also, Rh-106, Cs-134 and Cs-137 were detected at the interface. The location was confirmed by Mn-54 and Co-60 activities. F8B-3 was scanned multispectrally to investigate the gross gamma spikes in the blanket region corresponding the the enriched UO_2 pellet and the Ta spacers.* Peaks in the Cs-134 and Cs-137 activity plots indicated migration of these isotopes to the relatively cool top and bottom ends of the fully enriched UO_2 pellet. The Cs at the top of this pellet appeared to be only on the lower side of the Ta spacer (i.e., next to the enriched UO_2), but the Cs on the bottom appeared to be on both sides of the spacer. Cesium-137 had also deposited on the two spacers separating the depleted UO_2 pellet from the natural UO_2 that was located midway between the enriched UO_2 pellet and the top of the fuel column. Diametral gamma scans on F8B-3 showed a smooth activity distribution with an approximate cosine curve profile and no indication of a central void. F8B-5 showed a flat diametral activity distribution indicating fission product migration radially to the outer regions of the fuel. Fuel rods F8B-17, -9 and -12 exhibited gamma diametral scans similar to that of F8B-5. Diametral scan of F8B-16 showed a dip at the center corresponding to the

---

* The upper blankets on all of the pellet fuel rods consisted of the following: 4 natural UO_2 pellets adjacent to the top of the mixed oxide fuel, then an 0.01 inch thick Ta spacer, a single depleted UO_2 pellet, another Ta spacer, 4 natural UO_2 pellets, a Ta spacer, a fully enriched UO_2 pellet, a final Ta spacer, and 3 natural UO_2 pellets at the top of the ceramic column. The nominal length of all insulator pellets is 0.25 inch. The post-irradiation gamma scans of some Ta spacers showed an apparent increase in thickness to 0.025-0.03 inch, which may be due to scanner slit width effects or to some transfer of Ta beyond its original surfaces.

as-fabricated hole in the annular pellet. F8B-12 was a vipac rod. Its gamma scans were quite different from the others. There were no clearly defined interfaces between blanket or insulator regions and the fuel according to the gross scan. A broad spike in the gross scan ∿0.25 inch (6 mm) wide was noted at the top of the fuel, and a dip in activity ∿0.75 in (19 mm) wide was noted about 0.83 in (21 mm) below the midplane. Isotopic scans were made over the enriched fuel column. The Cs-137 activity plot showed Cs-137 had migrated to both ends of the fuel. A broad region of high Cs-137 activity at the top of the blanket indicated a considerable amount of Cs-137 had migrated and possibly penetrated the stainless steel wool located at the top of the ceramic column. A large broad dip in the Cs-137 activity below the midplane was noted. The Zr-95/Nb-95 gamma scan and the F8B-12 radiographs, however, did not show any corresponding fuel density variation. Small peaks observed at about the location of the top spacer on the extensometer were investigated and Co-60 was found to be the only isotope contributing any significant activity.

c. Dimensional Measurements

Post-irradiation diameter profiles were determined for the de-encapsulated rods. The optical profilometer was used for all rods except F8B-5.* Measurements were made for four orientations (0°, 45°, 90°, 135°). Circumferentially averaged diameters for 0.25 inch length increments (1.0 inch for F8B-5*) are shown in Figures 3-9 through 3-14. Local cladding diameter increases along the fueled length were determined by measuring the difference between the profilometry values as measured above and the unirradiated average diameter. Pre-irradiation profilometry was performed continuously over the length of these rods with a mechanical profilometer. The summary of cladding diameter measurements is shown in Table 3-11. It is surprising that the cold worked Type-304 cladding had the greatest diameter change and I-800 the least. Cold worked F8B-5 also had the highest fuel density, but the lowest fuel density rods did not necessarily have the smallest

---

* F8B-5 could not be measured optically because of a slight bend 10cm(4 inches) from the bottom. It was measured with a micrometer precise to 0.0005 inch at one inch intervals at 0° and 90° orientations.

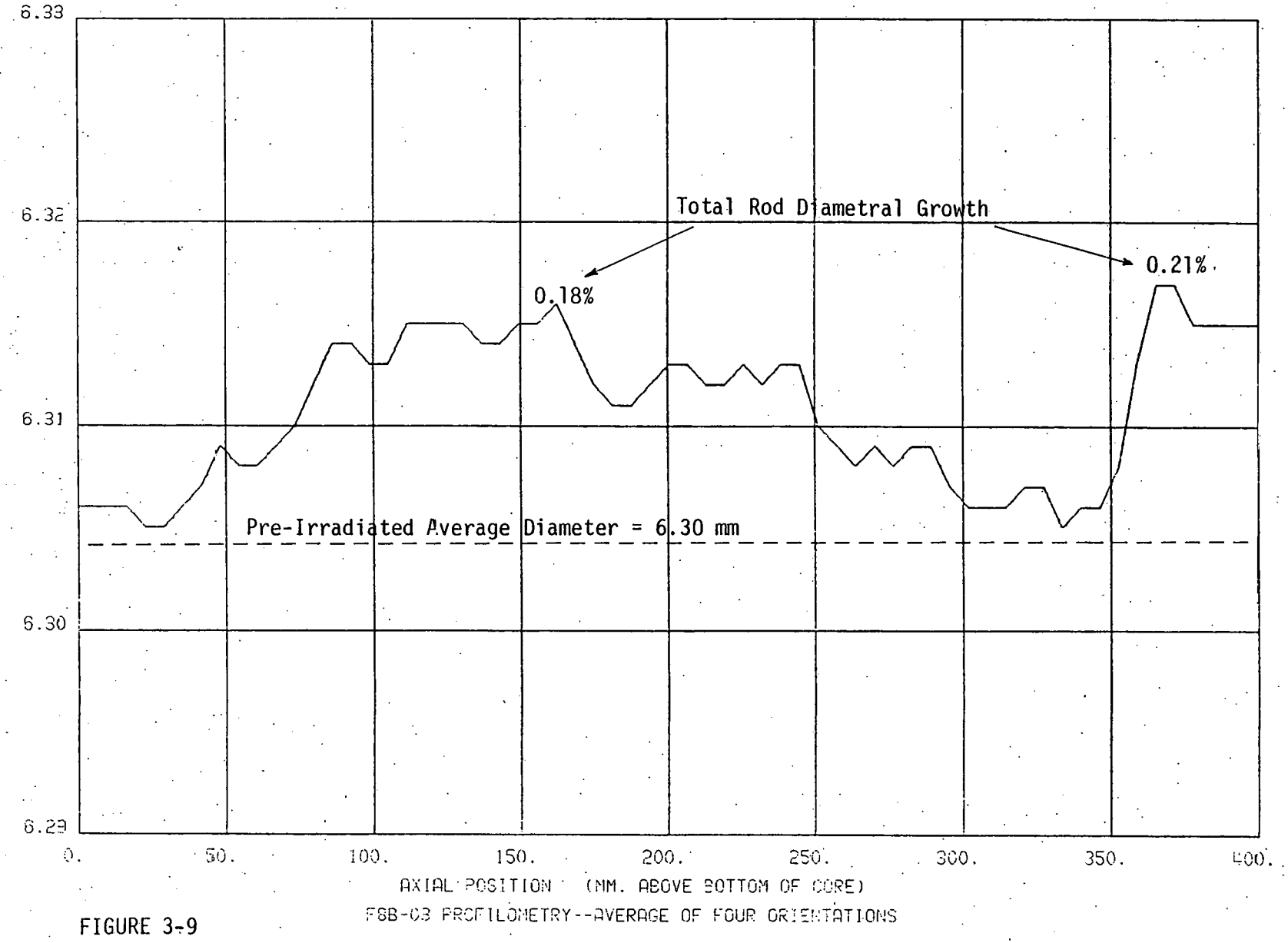
6.33
6.32
6.31
6.30
6.29
FUEL ROD DIAMETER (MM.)
Total Rod Diametral Growth
0.18%
0.21%
Pre-Irradiated Average Diameter = 6.30 mm
0.
50.
100.
150.
200.
250.
300.
350.
400.
AXIAL POSITION (MM. ABOVE BOTTOM OF CORE)
FSB-03 PROFILOMETRY--AVERAGE OF FOUR ORIENTATIONS

FIGURE 3-9

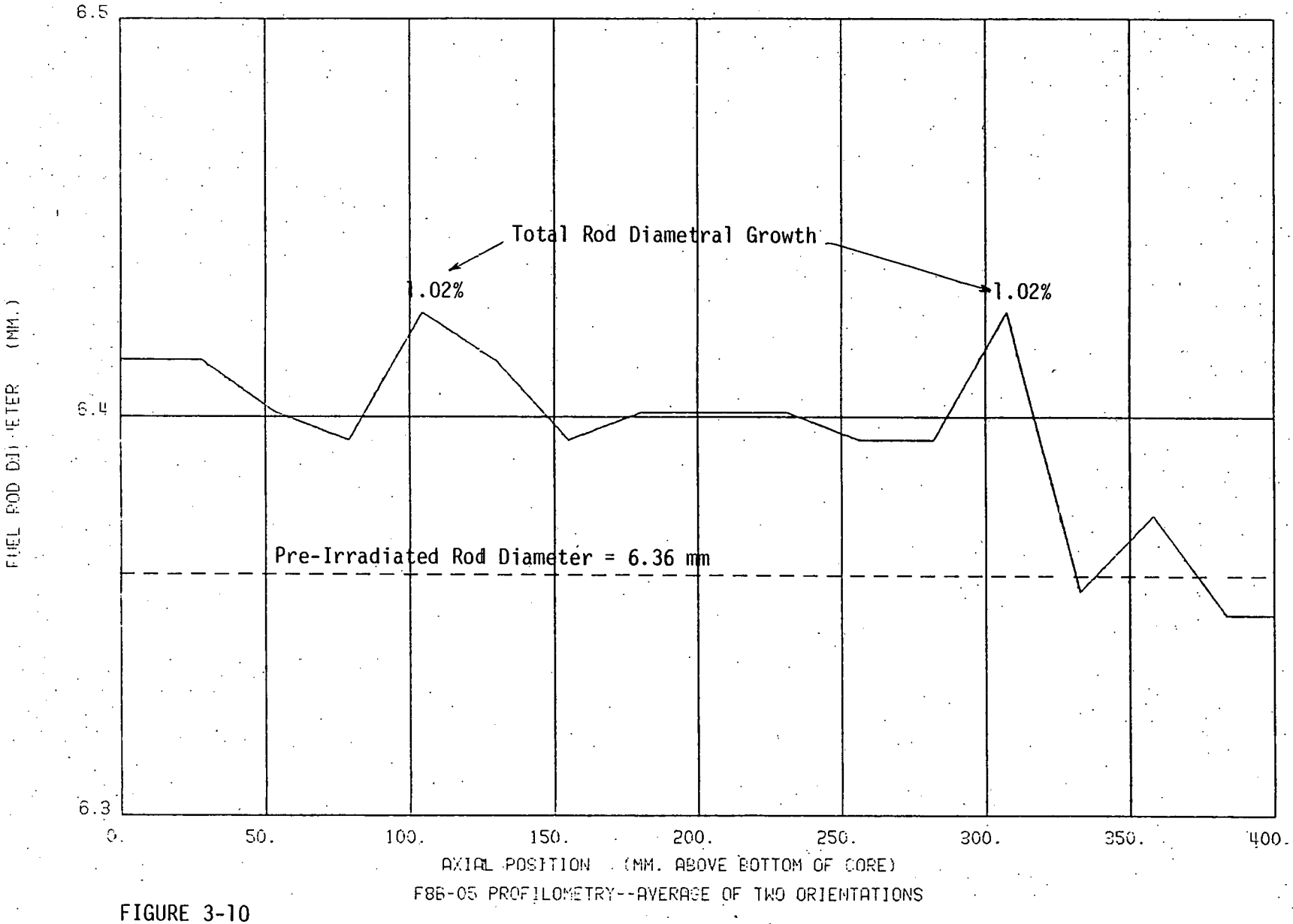
6.5
6.4
6.3
FUEL ROD DIAMETER (MM.)
Total Rod Diametral Growth
1.02%
1.02%
Pre-Irradiated Rod Diameter = 6.36 mm
0.
50.
100.
150.
200.
250.
300.
350.
400.
AXIAL POSITION (MM. ABOVE BOTTOM OF CORE)
F86-05 PROFILOMETRY--AVERAGE OF TWO ORIENTATIONS

FIGURE 3-10

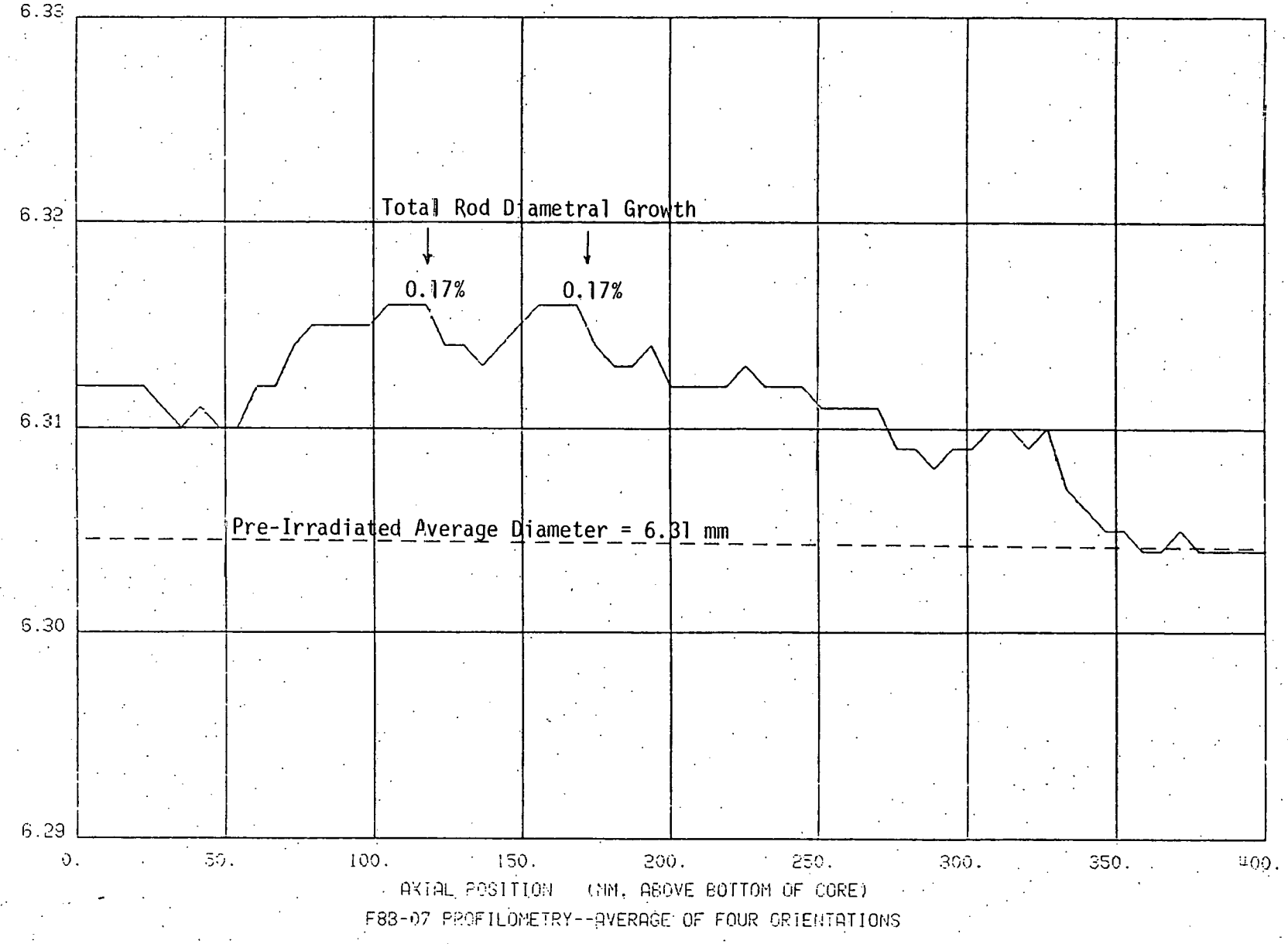
6.33
6.32
6.31
6.30
6.29
Total Rod Diametral Growth
0.17%
0.17%
Pre-Irradiated Average Diameter = 6.31 mm
FUEL ROD DIAMETER (MM.)
0.
50.
100.
150.
200.
250.
300.
350.
400.
AXIAL POSITION (MM. ABOVE BOTTOM OF CORE)
F88-07 PROFILOMETRY--AVERAGE OF FOUR ORIENTATIONS

FIGURE 3-11

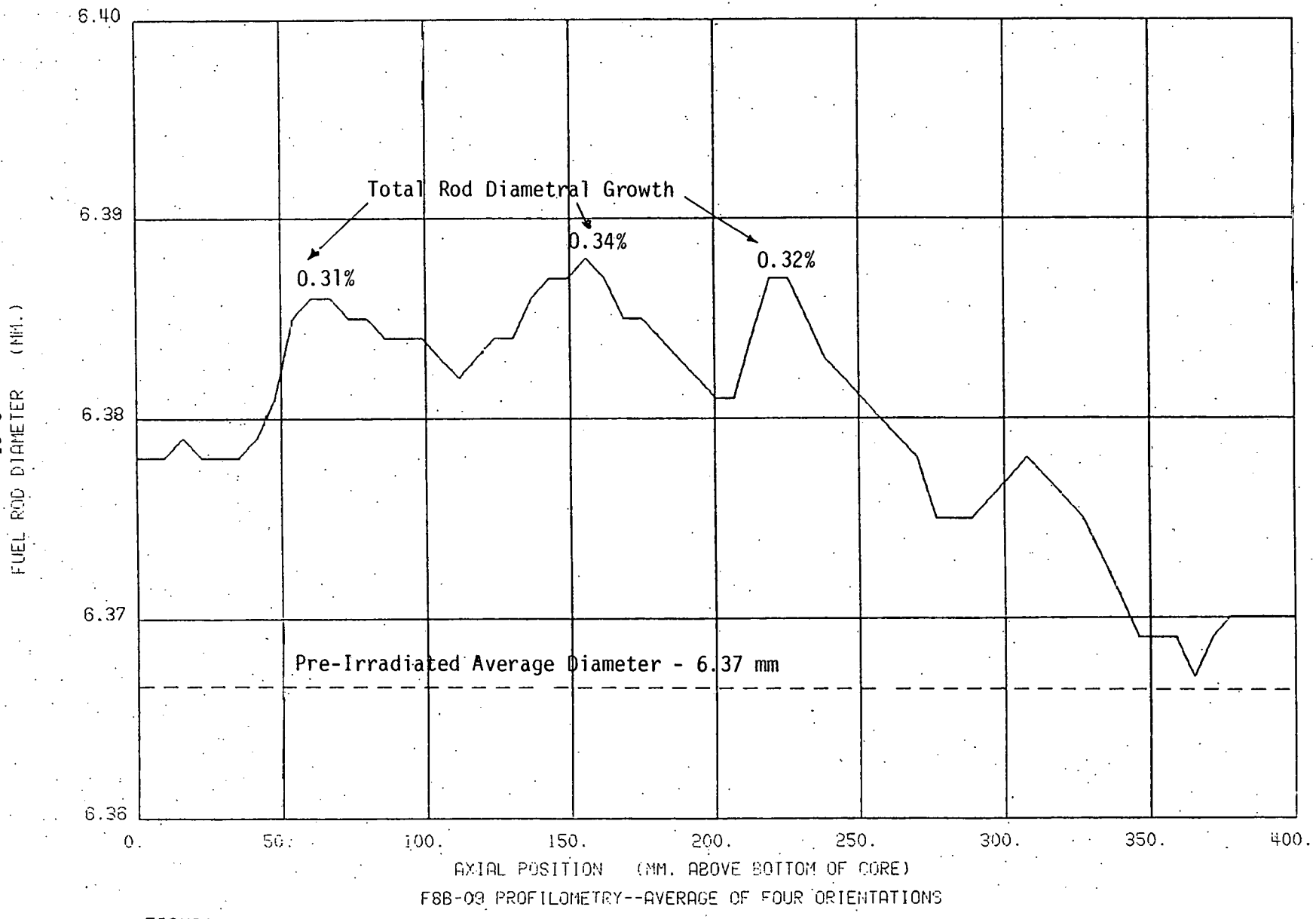
6.40
6.39
6.38
6.37
6.36
FUEL ROD DIAMETER (MM.)
Total Rod Diametral Growth
0.31%
0.34%
0.32%
Pre-Irradiated Average Diameter - 6.37 mm
0.
50.
100.
150.
200.
250.
300.
350.
400.
AXIAL POSITION (MM. ABOVE BOTTOM OF CORE)
F8B-09 PROFILOMETRY--AVERAGE OF FOUR ORIENTATIONS

FIGURE 3-12

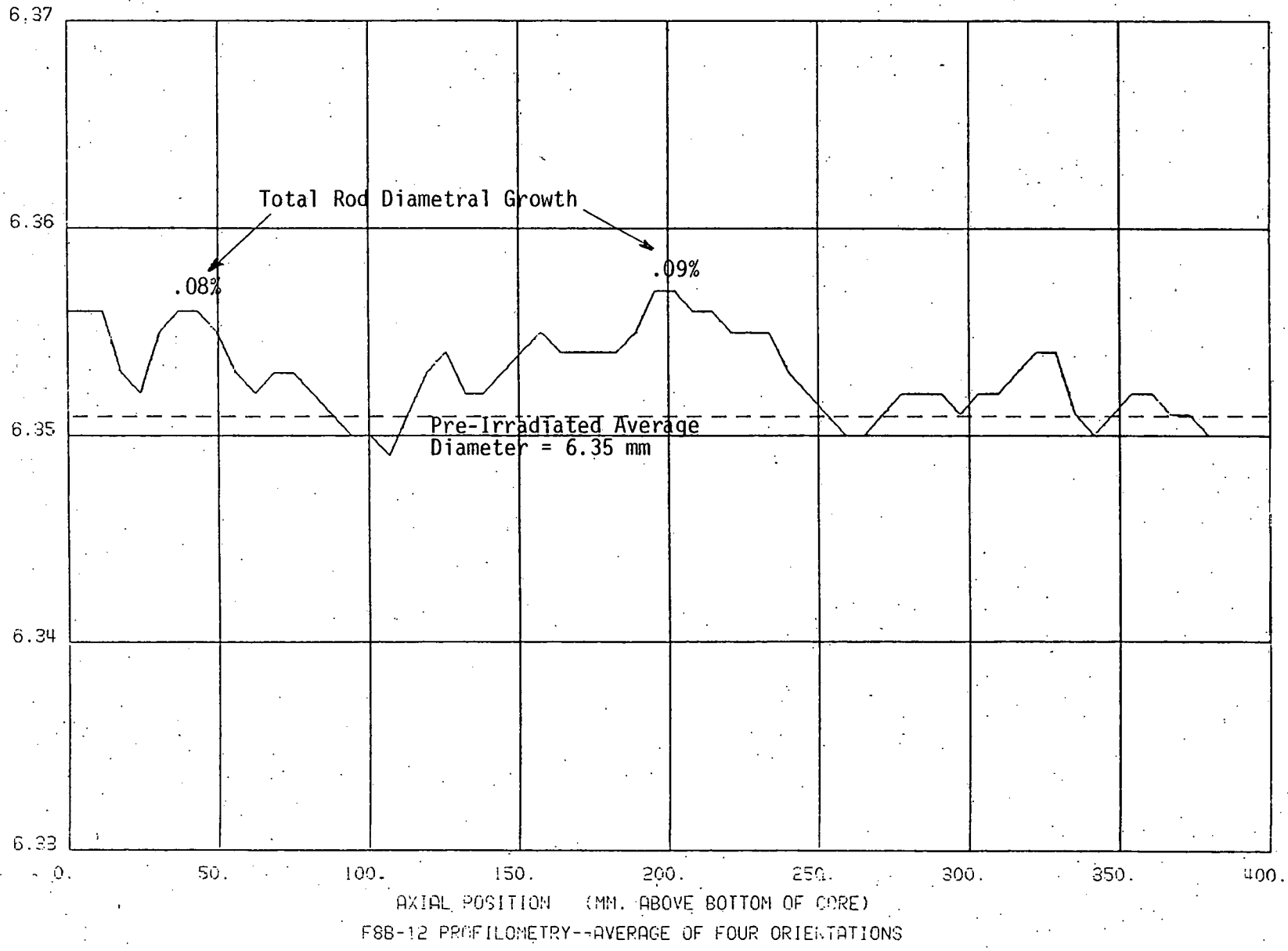
6.37
6.36
6.35
6.34
6.33
Total Rod Diametral Growth
.08%
.09%
Pre-Irradiated Average
Diameter = 6.35 mm
FUEL ROD DIAMETER (MM.)
0.
50.
100.
150.
200.
250.
300.
350.
400.
AXIAL POSITION (MM. ABOVE BOTTOM OF CORE)
F8B-12 PROFILOMETRY--AVERAGE OF FOUR ORIENTATIONS

FIGURE 3-13

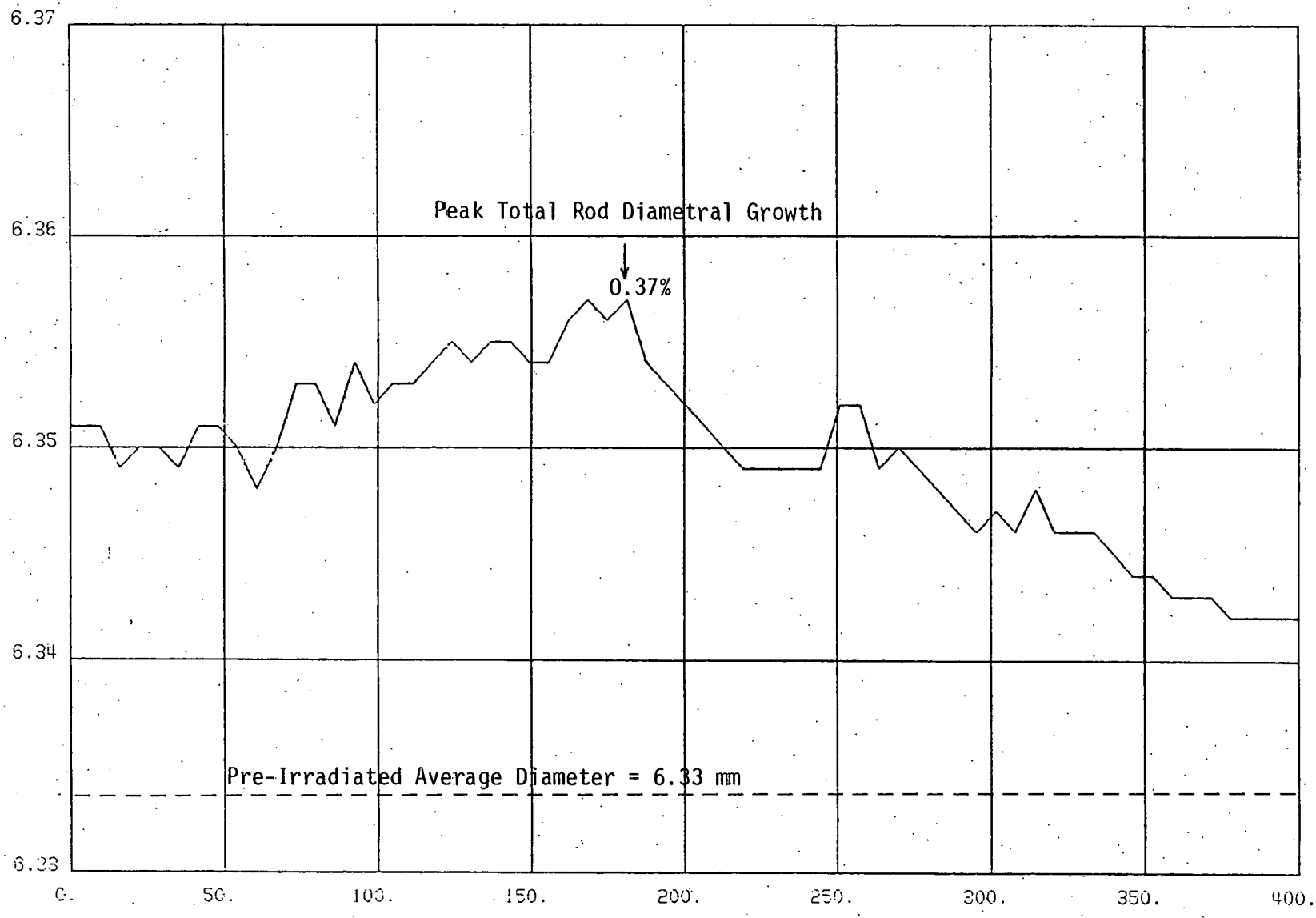
6.37
6.36
6.35
6.34
6.33
Peak Total Rod Diametral Growth
0.37%
Pre-Irradiated Average Diameter = 6.33 mm
FUEL ROD DIAMETER (MM.)
0.
50.
100.
150.
200.
250.
300.
350.
400.
AXIAL POSITION (MM. ABOVE BOTTOM OF CORE)
F8B-16 PROFILOMETRY--AVERAGE OF FOUR ORIENTATIONS

FIGURE 3-14

TABLE 3-11

CLADDING DIAMETER MEASUREMENTS

Fuel Rod	Cladding	In X117A?	Smeared Density (%)	Peak Burnup (%)	Peak Fast Fluence ($n/cm \times 10^{-22}$)	Diameter Increase %
F8B-3	I800	Yes	88.0	6.06	2.50	0.01 - 0.18
F8B-5	304CW	No	90.5	5.11	1.89	0.51 - 1.02
F8B-7	I800	Yes	88.0	5.73	2.18	0 - 0.17
F8B-9	316	No	83.4	6.63	3.09	0.01 - 0.34
F8B-12	I800	No	83.2V	6.20	2.70	0 - 0.09
F8B-16	304A	Yes	87.4	5.92	2.33	0.14 - 0.37

diameter increase. There appeared to be no correlation between diameter increase and whether or not the X117A overpower was applied.

Immersion density measurements were used to study the contribution of cladding swelling (assumed to be isotopic and equal to one-third of the total volumetric change) to the total rod diametral growth. Results of these measurements are shown in Tables 3-12 and 3-13. Surprisingly, the volume increases in Type-304 cold worked (1-3%) were substantially greater than in the other types. The I-800 and annealed Type-316 had cladding volume increases of about one-half of one percent. The slight volume decreases at the top of some rods (<0.1%) are well within the expected measurement errors.

The inelastic strains* in F8B-3, -7, -12, which are clad in I-800, were less than the $\pm$0.08% (0.0002 inch) precision of the measurement methods. This is also true of the Type-316 annealed clad rod (F8B-9) at the top and bottom of the fuel column; but there was a small significant mechanical strain (0.16%) at center. The cold worked Type-304 (F8B-5) had an apparent compressive strain (0.35%) at fuel center and a fairly large mechanical tension strain (0.59%) at the top. The compression is probably not real but a consequence of anisotropic dimensional changes due to void swelling. That the effect appeared only in the cold worked Type-304 cladding seems reasonable in view of the necessarily directionally dependent nature of the tube drawing process.

Fuel column length changes are shown in Table 3-14. These values were calculated using the activity transition locations on the gross gamma scans. Comparisons between the fuel length and rod diameter changes

---

* "Inelastic Strain" = Total Diameter Increase -1/3 (cladding density change).

TABLE 3-12

LOCAL CLADDING DENSITY MEASUREMENTS AND CLADDING SWELLING VALUES

Fuel Rod Section	Cladding	Post-Irradiation Density (gm/cm^2)	Pre-Irradiation Density (gm/cm^2)	Volume Swelling[a] (%)	Cladding Void Swelling[b] (%)
F8B-3 E	I800	7.938	7.970	0.40	0.13
H	I800	7.954	7.970	0.20	0.07
F8B-5 E	304CW	7.634	7.863	2.91	0.97
H	304CW	7.762	7.863	1.28	0.43
F8B-7 E	I800	7.922	7.970	0.60	0.20
H	I800	7.971	7.970	-0.01	0.00
F8B-9 C	316	7.921	7.972	0.64	0.21
G	316	7.929	7.972	0.54	0.18
J	316	7.938	7.972	0.43	0.14
F8B-12E	I800	7.955	7.970	0.19	0.06
H	I800	7.977	7.970	-0.09	-0.03
F8B-16E	304A	7.832	(c)		
H	304A	7.869	(c)		

a. Total volumetric swelling ($\Delta V/V$) was calculated using the equation: $\Delta V/V_o = (\rho_o - \rho_f)/\rho_f$ where V = Volume Change V_o = Original Volume ρ_o = original density and ρ_f = final density

b. Diametral cladding void swelling was assumed to be isotropic and calculated as one-third of the total volumetric swelling.

c. Density of unirradiated F8B-16 (304A) not available.

TABLE 3-13

LOCAL ROD DIAMETRAL GROWTH AND CLADDING SWELLING MEASUREMENTS

FUEL ROD SECTION	AXIAL LOCATION mm	CLADDING	CALCULATED LOCAL BURNUP (%)	LOCAL FLUENCE ($n/cm^2 X 10^{22}$)	LOCAL DIAMETER INCREASE (%)	CLADDING VOID SWELLING (%)	MECHANICAL[b] STRAIN (%)
F8B-3E	166	I800	6.05	2.49	0.18	0.13	0.05
H	321	I800	5.85	2.41	0.04	0.07	-0.03
F8B-5E	147	304CW	5.10	1.89	0.62	0.97	-0.35
H	342	304CW	4.29	1.59	1.02	0.43	0.59
F8B-7E	149	I800	5.72	2.17	0.17	0.20	-0.03
H	303	I800	5.55	2.11	0.07	0.00	0.07
F8B-9C	21	316	5.70	2.66	0.18	0.21	-0.03
G	166	316	6.63	3.09	0.34	0.18	.16
J	305	316	5.60	2.61	0.18	0.14	0.04
F8B-12E[c]	166	I800	6.20	2.70	0.05	0.06	-0.01
H	318	I800	5.21	2.27	0.03	-0.03	0.06
F8B-16E	147	304A	5.91	2.33	0.37	(d)	(d)
H	319	304A	5.74	2.26	0.22	(d)	(d)

(a) Mechanical swelling is defined as: $\Delta V/3V$ per Table 3-12.

(b) Total diameter increase -cladding void swelling. The term "Inelastic Swelling" is sometimes used, a confusing term since elastic behavior is not involved and incorrect because void swelling is also not elastic.

(c) Vibratorily compacted fuel.

(d) Density change not yet available for F8B-16 (304A).

TABLE 3-14

FUEL COLUMN LENGTH CHANGES

Fuel Rod	Cladding	Smeared Density (%)	Mean Gap (mils)	In X117A?	Length After Irradiation (cm)	Length Before Irradiation (cm)	Length Increase (%)	Maximum Diameter Increase (%)
F8B-3	I800	88.0	8.1	Yes	34.96	34.47	1.44	0.18
F8B-5	304CW	90.5	4.5	No	34.65	34.34	0.90	2.62
F8B-7	I800	88.0	5.1	Yes	34.37	34.28	0.24	0.17
F8B-9	316	83.4	3.0	No	34.51	34.40	0.30	0.34
F8B-12*	I800	83.2*	*	No	33.97	34.12	-0.42	0.09
F8B-16	304A	87.4	5.2	Yes	34.70	34.38	0.92	0.37

*Vibratorily compacted Fuel

indicate that the fuel swelling is irregularly anisotropic. This was especially true of cold worked F8B-5 which also showed evidence of anisotropy in the diameter increase data.

d. Fission Gas

The volume of capsule and rod plenum gas was determined by puncturing and expanding the gases into an evacuated chamber of known volume where the pressure rise was measured. Theoretical fission gas generation was calculated assuming a yield of 0.254 noble gas atoms per fission and using calculated burnup. A summary of the gas collected is shown in Table 3-15. The release fractions ranged from 0.35 to 0.67. These values seem fairly low, and they also vary substantially from rod to rod. If measured burnup values had been used, the release fractions would have been lower and more variable. Results of mass spectrographic analyses are shown on Tables 3-16 and 3-17. The results of rod gas analyses are normal, and the capsules contained no Xe or Kr to confirm that there was not the tiniest breach of the cladding. Except for rod F8B-12, however, the capsules were evacuated during fabrication and exhibited only traces of a contaminated He-Ar mixture at 10 to 16 torr pressure (1.4 - 2.0 kpa).

e. Optical Microscopy

Microscopy samples were prepared from 2-3 sections of each fuel rod. Transverse cross sections were taken at about the peak flux region and longitudinal sections at the top of the fuel. None of the sections examined exhibited a central void or any columnar grain growth. Cracks within pellets were observed. All of the longitudinal sections of pellet fueled rods showed inter-pellet gaps that were still well defined, as were the dished ends of the F8B-7 pellets. The vipac fuel of the F8B-12 rod was highly cracked. Measurements of fuel diameters, gap sizes and cladding thickness were made from montages of photomicrographs at 50 diameters magnification. The gap measurements are shown on Table 3-18. Except for sections at the top of rods F8B-3 and F8B-5, the hot gaps were essentially closed by the end of the irradiation.

TABLE 3-15

FISSION GAS RELEASE

Fuel Rod	Axial Average Burnup (%)	Fission Gas Collected (cc, STP)	Fission Gas Generated[a] (cc, STP)	Fission Gas Released (%)	Measured-Calculated Peak Burnup Discrepancy[b] %
F8B-3	5.46	75.0	95.3	67.3	10.9
F8B-5	4.57	38.5	80.2	35.7	8.9
F8B-7	5.16	50.0	89.5	43.6	7.3
F8B-9	5.94	65.9	98.2	55.9	2.5
F8B-12	5.56	58.0	90.8	51.2	3.8
F8B-16	5.34	50.9	92.7	43.3	11.8

a) At 0.254 fission gas atoms (Xe + Kr) per fission and calculated average burnup values from the burnup code.

b) See Table 3-19.

TABLE 3-16

F8B GAS ANALYSES AT 6% BURNUP

Rod/ Capsule	Pressure[a] Std. Temp. ATM	PSI	Total Gas Collected (g-moles)	Measured Void Volume, STP cm^3	Gas Composition (mole %) H_2	He	N_2/CO	O_2	Ar	Kr	Xe
F8B-3											
Rod	7.5	110	3.35×10^{-3}	9	-	14.5	<0.02	<0.02	<0.02	11.1	74.4
Capsule	.017	.26	7.0×10^{-6}	10	7	39	1	<0.2	54	<0.02	<0.02
F8B-5											
Rod	3.9	57	1.72×10^{-3}	9	-	25.6	<0.02	<0.02	<0.02	9.8	64.5
Capsule	.014	.21	5.8×10^{-6}	10	5	26	0.6	<0.2	68	<0.02	<0.02
F8B-7											
Rod	5.0	73	2.23×10^{-3}	7	-	21.8	<0.02	<0.02	<0.02	10.3	67.9
Capsule	.020	.29	6.1×10^{-6}	10	6	26	0.8	<0.2	67	<0.02	<0.02
F8B-9											
Rod	6.0	88	2.94×10^{-3}	8	-	16.6	<0.02	<0.02	<0.02	10.8	72.6
Capsule	.019	.27	6.6×10^{-6}	11	7	36	0.2	<0.2	57	<0.02	<0.02
F8B-12											
Rod	5.3	78	2.59×10^{-3}	10	-	19.9	<0.02	<0.02	<0.02	10.5	69.6
Capsule	.42	6.1	1.86×10^{-4}	11	-	98.7	0.03	<0.02	1.2	<0.002	<0.002
F8B-16											
Rod	5.1	75	2.27×10^{-3}	8	-	21.0	<0.02	<0.02	<0.02	10.3	68.6
Capsule	.017	.25	6.0×10^{-6}	10	8	29	0.2	<0.2	63	<0.02	<0.02

(a) Using measured void volumes.

TABLE 3-17

FISSION GAS ISOTOPICS, PERCENT

Rod Number	Kr-83	Kr-84	Kr-85	Kr-86	Xe-128	Xe-129	Xe-130	Xe-131	Xe-132	Xe-134	Xe-136
F8B-3	15.7	27.8	6.0	50.5	-	0.01	0.03	15.2	22.0	34.2	28.6
F8B-5	15.6	27.7	5.96	50.7	0.01	-	0.03	15.2	21.7	34.3	28.7
F8B-7	15.6	27.7	6.0	50.7	-	0.01	0.03	15.1	21.8	34.3	28.7
F8B-9	15.7	27.7	6.0	50.6	0.01	-	0.03	15.2	21.9	34.1	28.8
F8B-12	15.7	27.6	6.0	50.7	0.01	-	0.03	15.3	21.9	34.1	28.7
F8B-16	15.6	27.6	6.0	50.7	0.01	-	0.03	15.1	21.9	34.2	28.8

TABLE 3-18

FUEL-CLADDING GAP MEASUREMENTS

Fuel Rod	Section	Axial Distance (mm)	Local Fast Fluence (a) ($n/cm^2 \times 10^{-22}$)	EOL Local Power (kW/m)	EOL Clad ID Temp. (°C)	Fuel-Cladding Gap		
						Post-Irrad. (mils)	Pre-Irrad. (mils)	Decrease (%)
F8B-3	D(T) (b)	154	2.49	28.1	517	0.6	8.2	93
	I(L) (b)	345	2.41	27.2	588	5.7	7.7	26
F8B-5	D(T) (b)	142	1.88	18.1	482	1.5	5.0	70
	I(L) (b)	342	1.53	14.7	546	3.3	4.9	33
F8B-7	B(L)	111	2.15	30.4	512	1.0	4.7	79
	D(T)	146	2.17	30.6	527	0.0	5.6	100
	I(L)	336	2.10	29.8	604	2.0	5.9	66
F8B-9	B(L)	85	2.56	16.5	427	1.4	4.2	67
	F(T)	153	3.08	19.8	495	0.3	3.6	92
	K(L)	339	2.50	16.2	560	1.9	3.7	49
F8B-12	D(T) (b)	153	2.70	18.7	487	(c)	-	-
	I(L) (b)	340	2.18	15.2	548	(c)	-	-
F8B-16	D(T)	143	2.32	29.0	516	0.6	5.0	88
	I(L)	342	2.25	28.2	593	1.5	4.8	69

(a) From bottom of core to midpoint of specimen for longitudinal specimen or to top of specimen (polished surface) for transverse section.

(b) These longitudinal sections were cut on planes slightly below or above the plane of the true diameter.

(c) F8B-12 contained vibratorily compacted fuel and insulator in the form of presintered granules. Thus the outer fuel surface is somewhat irregular, both before and after irradiation. There appeared, however, to be no gap opening during irradiation. There were significant areas where the fuel was in contact with the cladding.

f. Burnup

Sections for burnup analysis were taken at about the peak flux region of all six rods and at the top of the fuel column of F8B-3 and -9. The burnup values reported by LASL were calculated using the old yield value of 0.0174 Nd-148 atom per fission. The values for experimental burnup shown in Table 3-19 were adjusted to the new yield of 0.0167 Nd-148 atom per fission. The calculated burnup values for the specimens near the axial midplane are 2-12% greater than the measured burnup. The two top of core specimens had calculated burnup that was -0.5 and +1.4% more than the measured value. It would appear, therefore, that the axial profile is not so flat as had been expected.

3.2.2 F9D

A selection of unencapsulated F9D rods from X058 is being examined at LASL after ∿8% burnup. The F9D-1 irradiation and HFEF examination at 14% burnup (X204) was described in Section 3.1.3.

3.3 BREACHED CLADDING

The post-irradiation examination of 16 encapsulated rods with breached cladding is continuing at LASL. A cladding breach was detected in the unencapsulated F11A experiment at the end of run 80A (see HIGH CLADDING TEMPERATURE IRRADIATIONS). The breach was in rod F11A-41 only. This was the highest cladding temperature rod.

3.4 HIGH CLADDING TEMPERATURE IRRADIATIONS

3.4.1 F10A, F10B, F10A-1 Experiments

Subassembly X121A (F10A-1, a reconstitution of nineteen F10A (X121) and F10B (X122) rods began irradiation in run 80. It has achieved approximately 9% burnup as of October 1976 (run 84 completed). The goal burnup of ∿11% is expected to be reached at the end of run 86 (January 1977). These are high cladding temperature (1300°F, 700°C) encapsulated rods. A small amount (0.001 to 0.002 inch, 25-50 μm) of fuel cladding chemical interaction was observed in rod F10B-2. This rod from X122 operated at ∿1250°F (680°C) to about 5% burnup. A topical report (GEAP-14133) covering the irradiation and post-irradiation examination of the 5% burnup F10A and F10B rods from X121 and X122 has been approved and is in the publication process.

TABLE 3-19

BURNUP ANALYSIS RESULTS

Fuel Rod Section	Axial Distance (mm) [a]	Measured Burnup (%) [b]	Calculated Burnup (%) [c]	% Difference
F8B-3C	138	6.77	6.03	10.9
G	308	5.85	5.88	-0.5
F8B-5C	126	5.53	5.04	8.9
F8B-7C	130	6.14	5.69	7.3
F8B-9E	138	6.75	6.58	2.5
I	301	5.70	5.78	1.4
F8B-12C	138	6.39	6.15	3.8
F8B-16C	127	6.28	5.54	11.8

(a) From bottom of core to midpoint of specimen.

(b) Except for Section G of F8B-3, the values reported by LASL used the old yield value of 0.0174 Nd-148 atom per fission in calculating the measured burnup. The values of measured burnup tabulated above were adjusted to the new yield for Nd-148 of 0.0167 per fission.

(c) As calculated by the 3URN-Code.

(d) Measured-calculated/measured (ICP-1050-1)

3.4.2 F11A Experiment

The F11A experiment is a high cladding temperature irradiation of unencapsulated mixed-oxide fuel rods in EBR-II. Thirty-seven rods in a MkJ-37 irradiation vehicle, designated subassembly X141, were loaded into row 6 of EBR-II for run 60. They were discharged following run 68 at a peak burnup of ~5 at.%. Interim examination showed no evidence of cladding breach. Three rods were shipped to LASL for destructive examination. The remainder, plus three F9E* rods, were reconstituted as subassembly X141A and loaded into row 6 for run 79. At the end of run 80A, fission gas activity appeared in the reactor cover gas, and EBR-II was shut down. Subassembly X141A was identified as the leaker by cover gas analysis corresponding to the F11A xenon gas tag. Subsequent gamma scanning of the plena showed F11A41 to be the only rod containing no fission gas. Visual examination showed no obvious defect in the cladding.

Diametral profilometry measurements were made of F11A-41 both during the interim examination and after cladding breach. The wire wrap was left in place so helical profilometry measurements were made ~90° either side of the wrap with the same pitch as the wire wrap. This is the usual interim examination procedure for wire wrapped rods at HFEF. These profilometry traces are reproduced in Figures 3-15 and 3-16. A substantial increase in cladding deformation is evident in the top 3 inches of the fuel column and in the blanket region. This is the region in which a breach might be expected to occur in a high cladding temperature rod. Whether this strain occurred before or after breach is of interest. Gross scanning of gamma activity after removal from the reactor showed no unusual activity peaks. Isotopic scans have not yet been made. The deformation may result from sodium ingress while the rod remained in the primary coolant or from fuel and/or sodium reaction during the water wash.

---

* The F9E rods were unirradiated spares similar to the F11A rod except they were not wire wrapped. Each F9E rod was positioned in the subassembly so that it was not adjacent to the duct wall or to any other F9E rod.

3.4.2.1 Post-Irradiation Examination of Three X141 Rods

Three rods (F11A-11, -23 and -28) were removed from the X141 subassembly after irradiation to ∿5% peak burnup and shipped to LASL for destructive examination. Some of the results of that examination are presented below.

All three rods are clad in AISI Type-316 but with different thermal treatments. The fabrication parameters are given in Table 3-20 and the irradiation conditions in Table 3-21.

3.4.2.2 Profilometry

Optical profilometry was performed at four rotational orientations and averaged to give the mean deformation. The traces are shown in Figures 3-17 through 3-19. Also shown in these figures are the pre-irradiation diameters and the corresponding irradiation-induced cladding density decreases. In this presentation the cladding swelling was assumed to be isotropic, and the calculations were based on pre-irradiation diameter measurements. The F11A cladding is seamless, and the variation of the pre-irradiation diameter in the fueled region is small (±0.0001 inch).

3.4.2.3 Cladding Density

Immersion density weighings were made on four 1/2-inch long sections from each rod. Results are given in Table 3-22. Although the fluence level is fairly low, the annealed cladding shows a peak swelling in the range (about 1050°F midwall) predicted by empirical correlations derived from non-fueled tests.[3-3] The peak swelling temperature for the carbide agglomerated cladding is substantially lower (about 925°F cladding midwall). The cold worked cladding shows slight swelling and slight densification. This densification has been observed in other GE experiments (F10A, F10B) at comparable cladding fluences and temperatures. The GE-FBRD current interpretation is that this magnitude of density increase (±0.2%) lies within the error band of measurement for irradiated (or unirradiated) samples.

TABLE 3-20

F11A FUEL ROD DESIGN PARAMETERS

Fuel Rod	Cladding Material	Mean Cladding OD (in.)	Mean Cladding Wall Thickness (in.)	Mean Fuel OD (in.)	Mean Pellet Density (%)	Smeared Density (%)	Minimum Fuel/Cladding Diametral Gap (mils)	O/M Ratio
F11A-11	316 Ann.	.2498	.0155	.2150	91.91	87.94	4.1	1.966
F11A-23	316 20%CW	.2503	.0150	.2151	92.24	88.05	4.8	1.968
F11A-28	316 CA(1)	.2503	.0153	.2151	92.07	87.97	4.7	1.969
F11A-41	316 20%CW	.2502	.0149	.2158	92.61	88.67	4.7	1.975

(1) Carbide agglomerated (solution annealed then 1650°F for 24 hours)

TABLE 3-21

F11A IRRADIATION CONDITIONS

Fuel Rod	Peak Linear Power (kW/ft) BOL	Peak Linear Power (kW/ft) EOL	Peak Cladding Temperature (°F) BOL	Peak Cladding Temperature (°F) EOL	End of Life Peak Burnup (%)	Peak Fast Fluence (10^{22} n/cm^2)
F11A-11	15.01	11.85	1304	1181	4.78	2.8
F11A-23	14.63	11.56	1192	1092	4.68	2.7
F11A-28	15.33	12.08	1215	1110	4.90	2.9

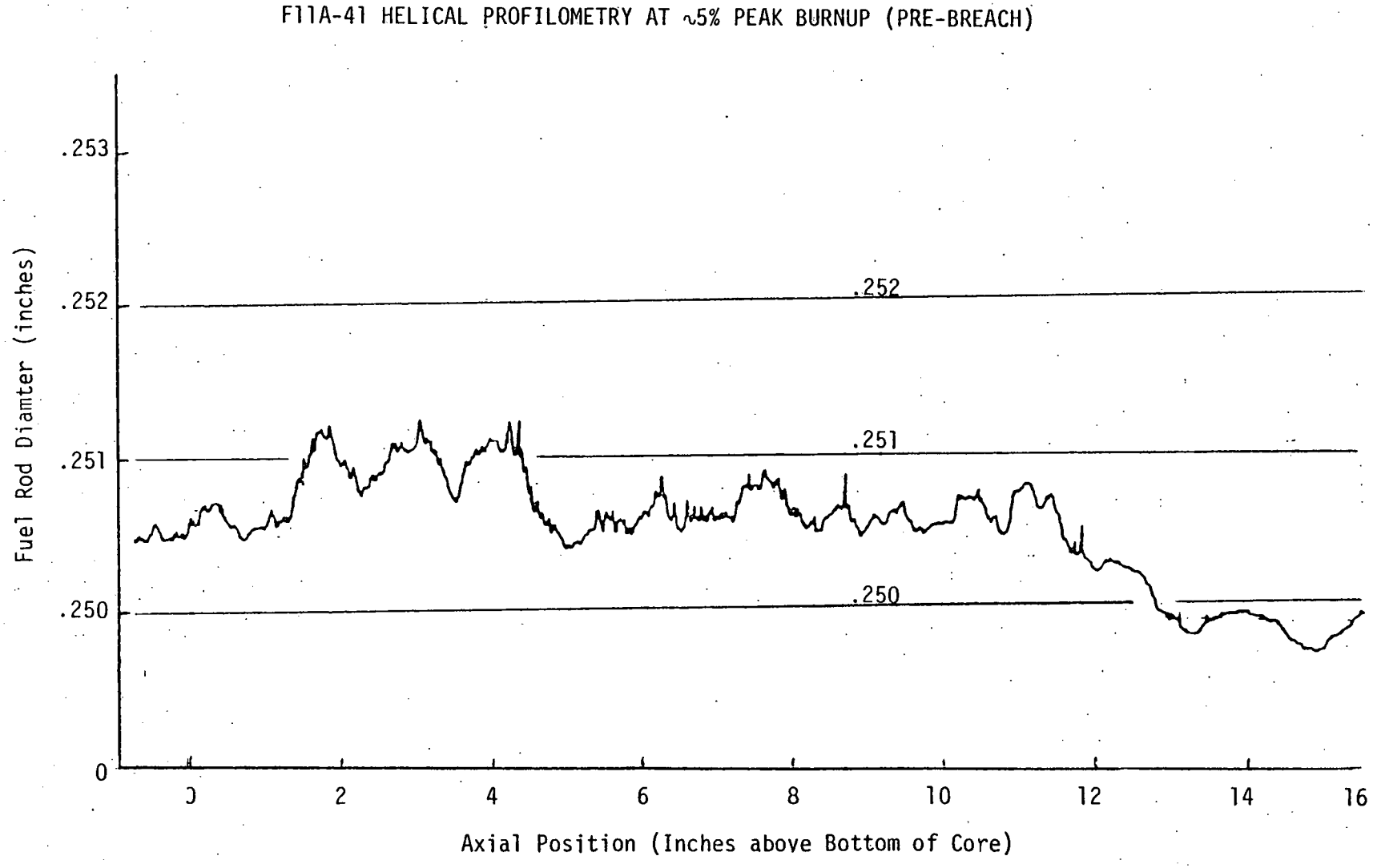
F11A-41 HELICAL PROFILOMETRY AT ∿5% PEAK BURNUP (PRE-BREACH)
Fuel Rod Diamter (inches)
.253
.252
.251
.250
0
.252
.251
.250
0
2
4
6
8
10
12
14
16
Axial Position (Inches above Bottom of Core)

FIGURE 3-15.

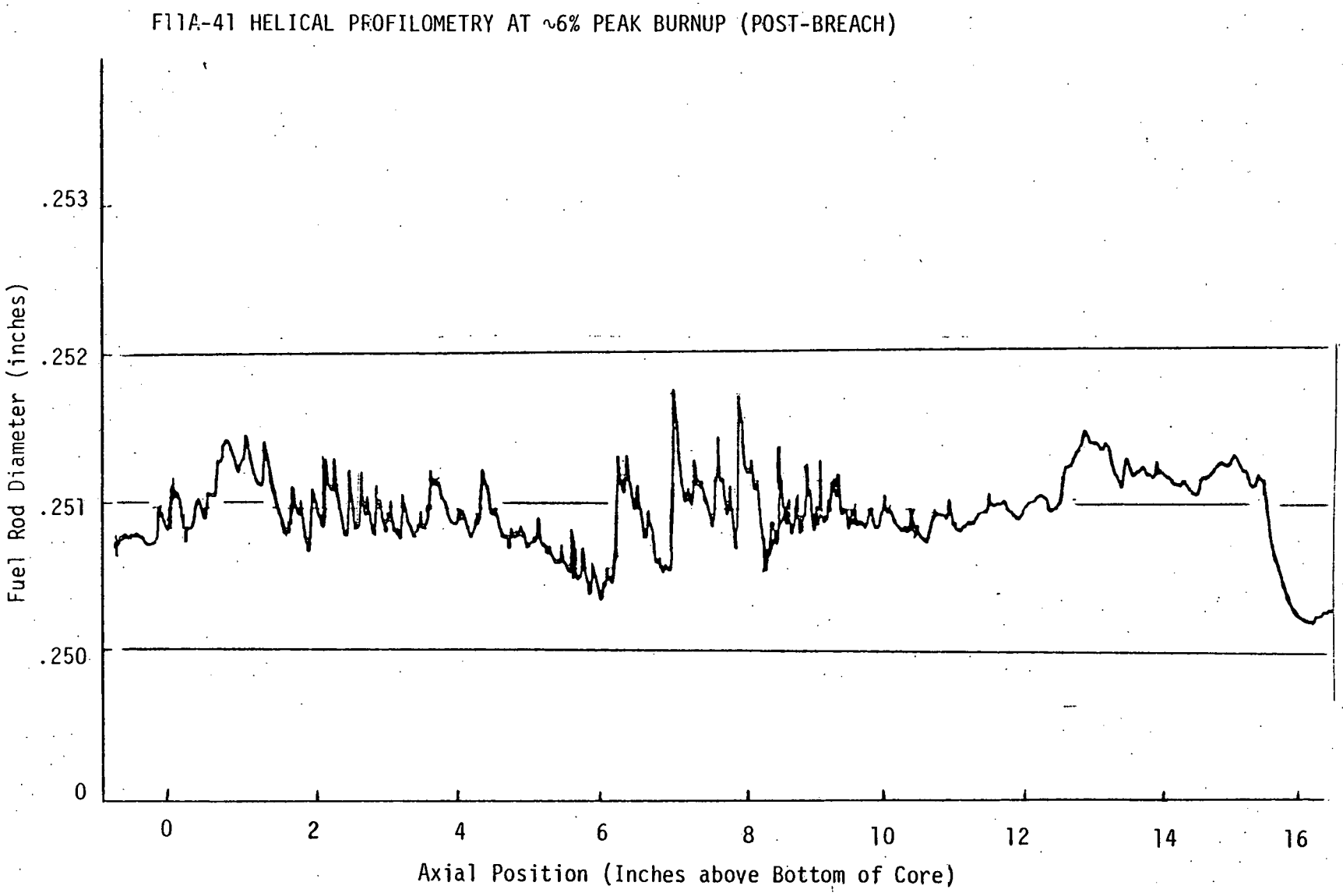
F11A-41 HELICAL PROFILOMETRY AT ~6% PEAK BURNUP (POST-BREACH)
Fuel Rod Diameter (inches)
.253
.252
.251
.250
0
0
2
4
6
8
10
12
14
16
Axial Position (Inches above Bottom of Core)

FIGURE 3-16

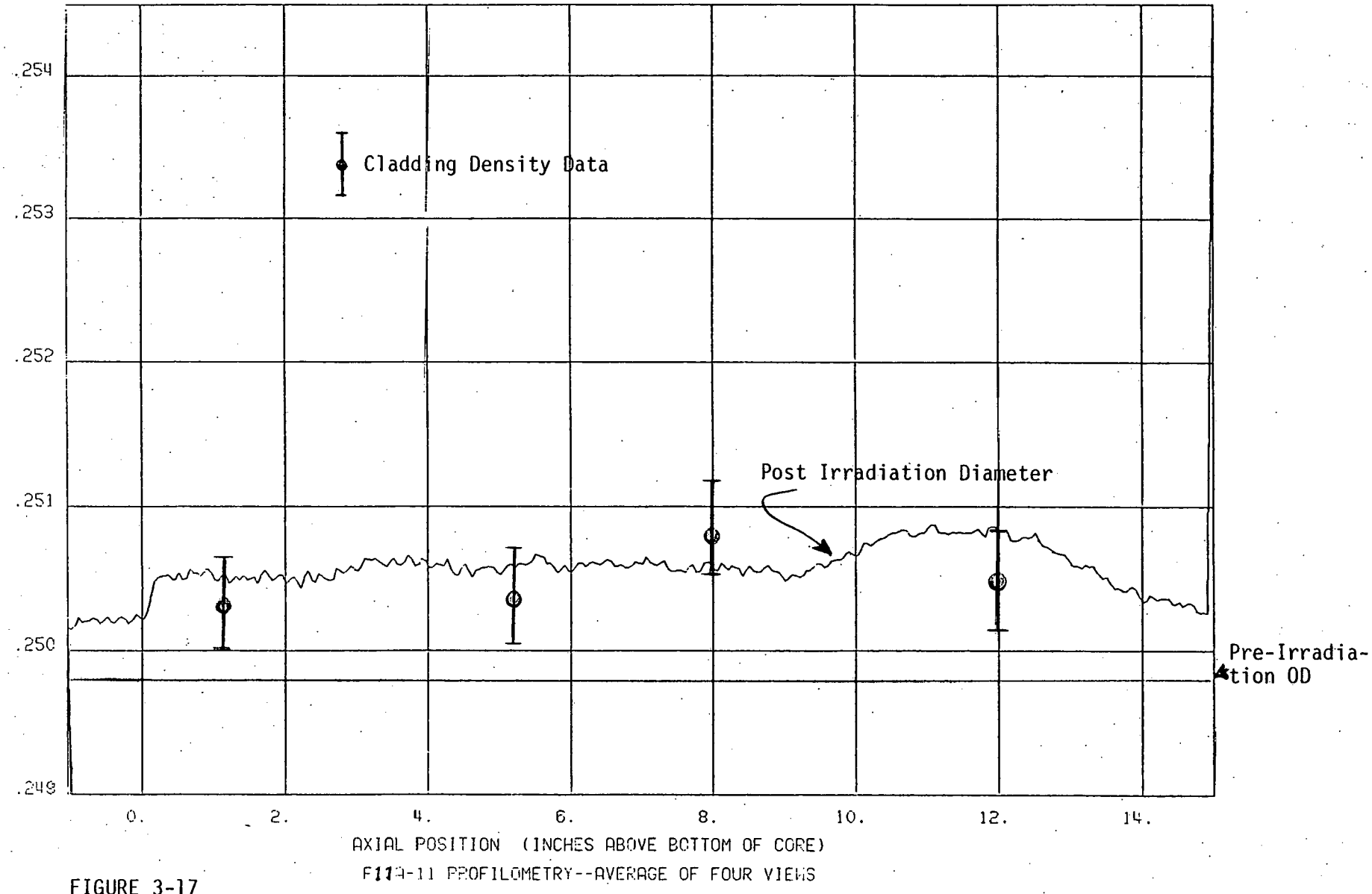

F119-11 PROFILOMETRY--AVERAGE OF FOUR VIEWS

FIGURE 3-17

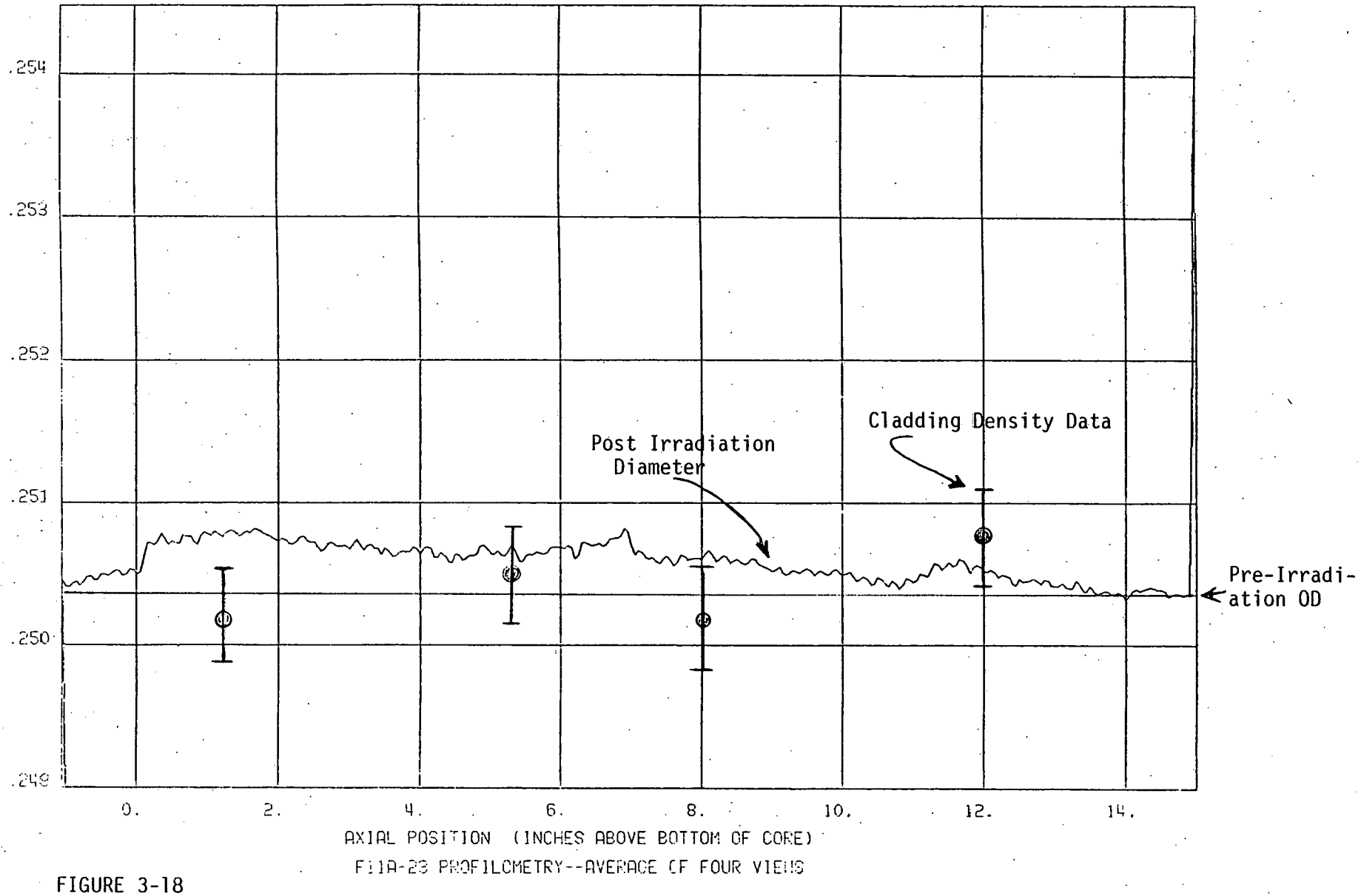
.254
.253
.252
.251
.250
.249
FUEL ROD DIAMETER (INCHES)
Post Irradiation Diameter
Cladding Density Data
Pre-Irradiation OD
0.
2.
4.
6.
8.
10.
12.
14.
AXIAL POSITION (INCHES ABOVE BOTTOM OF CORE)
FIIA-28 PROFILOMETRY--AVERAGE OF FOUR VIEWS

FIGURE 3-18

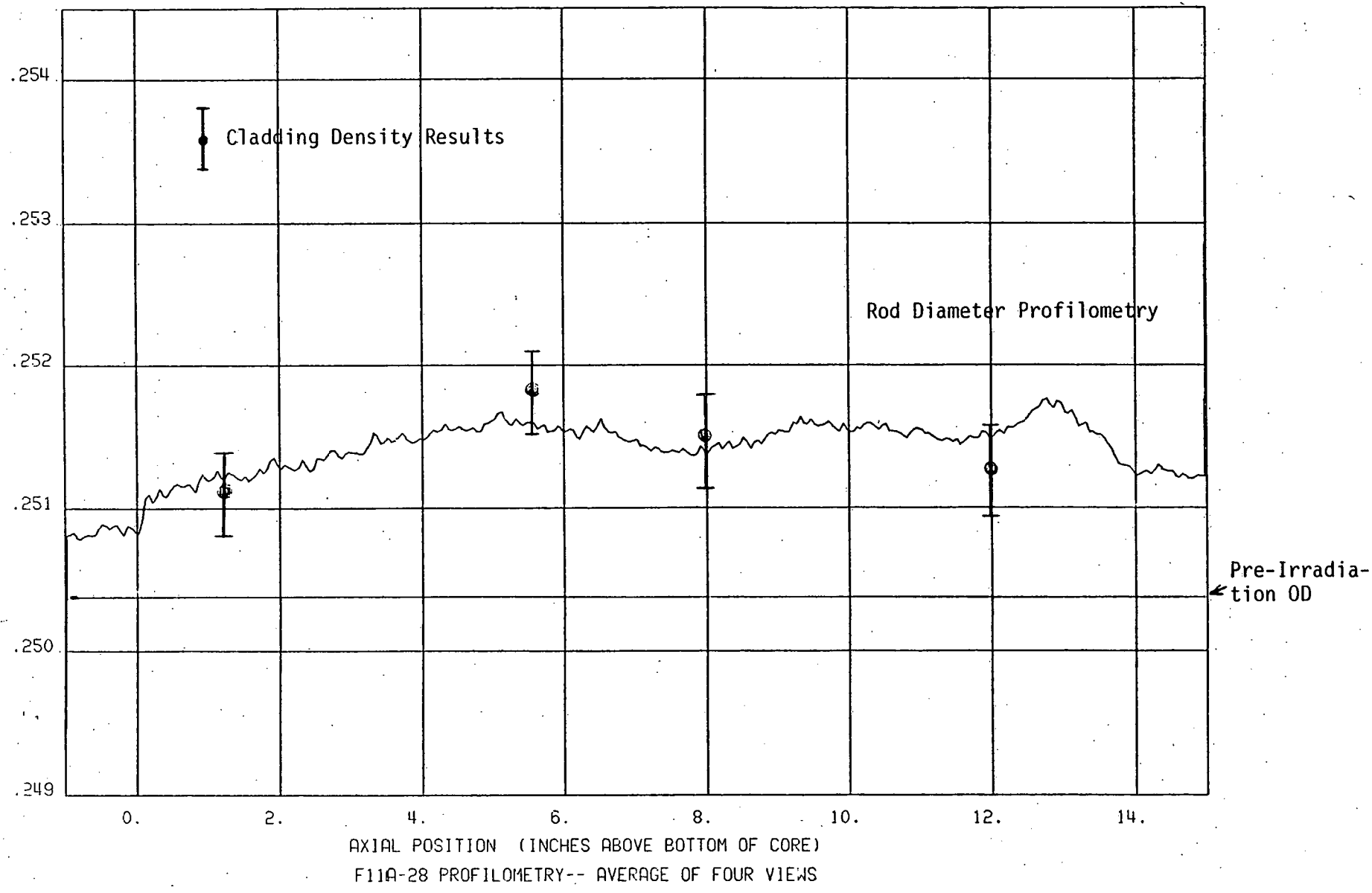
.254
.253
.252
.251
.250
.249
Cladding Density Results
Rod Diameter Profilometry
Pre-Irradiation OD
0.
2.
4.
6.
8.
10.
12.
14.
FUEL ROD DIAMETER (INCHES)
AXIAL POSITION (INCHES ABOVE BOTTOM OF CORE)
F11A-28 PROFILOMETRY-- AVERAGE OF FOUR VIEWS

FIGURE 3-19

TABLE 3-22

F11A IMMERSION DENSITY

Rod	Section	Cladding Condition	Elevation Above Bottom of Core (in)	Cladding Midwall Temp.(F°) BOL	Cladding Midwall Temp.(F°) EOL	Fast Fluence ($n/cm^2 \times 10^{-22}$)	Measured Density Decrease
F11A-11	E	Annealed	1-1/4	822	798	1.71	0.63
	J	Annealed	5-1/4	981	924	2.23	0.70
	O	Annealed	8	1086	1007	2.22	1.27
	R	Annealed	12	1216	1109	1.73	0.90
F11A-23	D	Cold Worked	1-1/4	814	790	1.64	-0.18
	J	Cold Worked	5-1/4	932	885	2.14	0.14
	O	Cold Worked	8	1011	948	2.13	-0.20
	R	Cold Worked	12	1111	1026	1.66	0.50
F11A-28	D	Carb. Agglom.*	1-1/4	820	796	1.77	0.13
	I	Carb. Agglom.	5-1/2	951	900	2.32	0.96
	N	Carb. Agglom.	8	1026	959	2.30	0.64
	Q	Carb. Agglom.	12	1130	1040	1.79	0.34

* Annealed +1650°F, 24 hrs.

3.4.2.4 Burnup

Three to five burnup samples about 1/2-inch long were taken from each rod. Isotope dilution mass spectroscopy was used to measure the burnup using Nd-148 as the fission monitor. Results are in Table 3-23. The calculated burnup values agreed fairly well with the measured burnup. The discrepancies were within +3, -4%, which verifies both the calculation of peak powers and the axial profile.

3.4.2.5 Optical Microscopy

Two transverse sections from each rod were prepared for photomicroscopy. Measurements of the fuel microstructural regions were made from photomosaics at 75 diameters. These measurements are reported in Table 3-24. The residual gap measurements indicate that the fuel was essentially touching the cladding at operating temperature. No micrographs showed substantial matrix attack of the cladding. Section T of F11A-11, ∿13 inches above the bottom of the core, showed ∿0.0018 inches of intergranular penetration (the maximum observed).

3.4.2.6 Conclusions

The post-irradiation examination results at 5% burnup (X141) showed normal conditions for the power and temperature levels involved. The diameter change at the top of rod F11A-41 between X141 and X141A (6% burnup) suggests that excessive creep deformation or fuel-cladding mechanical interaction may have contributed to the cladding breach.

3.5 THERMAL PERFORMANCE IRRADIATIONS

3.5.1 F20 Power to Melt Experiment

The destructive examination of twenty-eight F20 rods is continuing at LASL. Detailed evaluations of the fuel microstructures, dosimetry, and irradiation conditions are proceeding at GE. The basis for the power and temperature calculations has been established for this experiment. Dosimetry, burnup and gamma scan data have been correlated with fission rate calculations to support

TABLE 3-23

F11A BURNUP PROFILES

Rod	Section	Elevation Above Bottom of Core (in)(a)	Burnup (%)(b)	Burnup (%)(c)	Calculated Burnup (%)	Percent Difference(d)
F11A-11	D	1.1	4.15	4.32	4.20	-2.8
	H	4.5	4.63	4.81	4.67	-2.9
	K	6.0	4.68	4.87	4.76	-2.2
F11A-23	F	3.0	4.25	4.42	4.38	-0.9
	K	6.0	4.50	4.68	4.66	-0.4
	P	8.9	4.33	4.50	4.54	+0.9
F11A-25	E	2.1	4.44	4.61	4.42	-4.1
	H	5.0	4.82	5.02	4.84	-3.6
	M	7.9	4.74	4.93	4.86	-1.4
	P	11.9	4.03	4.19	4.31	+2.9

(a) Inches above bottom of core of center of 1/2 inch section.

(b) Nd-148 yield in Nuclear Science Engineering 42,191 (1970) (1.61 Nd-148/100 fissions).

(c) Nd-148 yield per ICP-1050-1(1975 (1.74 Nd-148/100 fissions).

(d) (Calculated-Measured)/measured per ICP-1050-1.

TABLE 3-24

MICROSTRUCTURAL REGION DIAMETERS

Rod	Section	Axial Location (Inches above Bottom of Core)	As-Fabricated Fuel/Cladding Diametral Gap (in)	Residual Diametral Gap (in)	Central Void (in)	Columnar Grain Growth (in)
F11A-11	I	4.7	.005	.002	.038	0.145
"	S	12.5	.005	.002	.021	0.125
F11A-23	G	3.2	.005	.001	.031	0.124
"	S	12.6	.005	.003	.018	0.128
F11A-28	J	5.7	.005	.002	.044	0.151
"	R	12.5	.005	.005(a)	.021	0.121

(a) The fuel-cladding gap in this section is filled with a material (probably a fission product) that etched darker than the fuel. Electron microprobe examinations will be made to determine the constituent elements.

this basis. The errors are considered to be less than 3%. About 100 microstructural specimens have been completed at LASL; microstructural measurements have been made at GE for approximately 50 specimens. A progress report (GEAP-14134) covering the available examination data has been approved and is in the publication process. Burnup measurements performed at GE-VNC on three samples are in good agreement with the LASL results. Additional burnup comparison specimens are being analyzed at ANL-West for both Nd and La fission product monitors.

3.6 RUN-TO-CLADDING BREACH IRRADIATIONS

3.6.1 F9C-1

The F9C-1 (X143A) experiment was discussed in Section 3.1.2 under HIGH BURNUP IRRADIATIONS.

3.6.2 F11A

The F11A experiment (X141, X141A, X141B) was discussed in Section 3.4.2 under HIGH CLADDING TEMPERATURE IRRADIATIONS. The soon-to-be reconstituted irradiation vehicle (X141B) has been proposed as a run-beyond-cladding breach experiment.

3.6.3 F9F

The F9F (X155) grid spaced irradiation vehicle has received full subassembly neutron radiography at TREAT. It will be disassembled during the first quarter, GFY77. The objectives of the grid spaced evaluation program will then have been achieved, but the rods should be available (at 11.8% peak burnup, 7.7×10^{22} n/cm^2 peak fast fluence) for further irradiation. It is planned to reconstitute these 0.23-inch diameter cold worked Type-316 rods as a run-to-cladding breach experiment.

3.7 SUBTASKS B AND C

Subtask B (Material Properties) and Subtask C (Data Evaluation) have been included in project 189 number SG009 for only one month during the current quarterly reporting period. Only Subtask A (Irradiation Testing) was discussed above. The technical progress in Subtasks B and C will be included in future reports of this program.

REFERENCES

3-1 Reference Fuel Studies First Annual Report February 1975 - January 1976, GEAP-14032-4 (February 1976).

3-2 J. E. Irvin: Nuclear Systems Materials Handbook, TID 26666 Correlation NSMH; SA316, 3304CE-D, Rev. 2, 4-16-75, Hanford Engineering Development Laboratory.

3-3 Nuclear Systems Materials Handbook, TID 26666, Rev. 5, 9-29-76, Hanford Engineering Development Laboratory, Richland, Washington.

MAJOR CONTRIBUTORS

N. T. Arcilla
L. A. Gatus
R. F.Hilbert
M. D. Mitchell
D. E. Plumlee
J. M. Rosa
C. L. Shearer
N. M. Tuttle
B. Levine